Title

Impacts of Fixed-End and Flexible Boundary Conditions on Seismic Response of Shallow Foundations on Saturated Sand in 1-g Shaking Table Tests

Journal
Geotechnical Testing Journal, 44(3)

ISSN
0149-6115

Authors
Jafarian, Y
Esmaeilpour, P
Shojaeemehr, S
et al.

Publication Date
2021-05-01

DOI
10.1520/gtj20200018

Peer reviewed

Impacts of fixed-end and flexible boundary conditions on seismic response of shallow foundations on saturated sand in 1g shaking table tests

Y. Jafarian[1*], P. Esmaeilpour[2], S. Shojaeemehr[3], H. Taghavizade[4], S. Rouhi[5], J.S. McCartney[6]

Abstract

A key consideration in physical modeling of seismic problems in geotechnical engineering is the impact of the model container boundaries on the soil layer response. The container boundaries may alter the stress-strain behavior from free-field conditions through the possible reflection of incident shear waves and generation of P-waves within the soil layers. In this study, 1g shaking table experiments were performed to evaluate the impacts of container boundary conditions on the response of saturated, loose sand layers subjected to harmonic base motions in (1) a free-field condition, (2) with a shallow foundation, and (3) with a shallow foundation supporting a single degree of freedom super-structure. The sand layers were formed in a newly-fabricated laminar shear container that can be converted to a rigid box by adding elements to the end walls. Acceleration, excess pore water pressure, and settlement measurements demonstrate that the rigidity of the container boundaries can have a major impact on seismic behavior of the models. In particular, the observed permanent settlement of the foundations increased by 58% to 115% in the soil models with fixed-end (or rigid) boundaries compared to those in soil models with flexible conditions. This was attributed to non-uniformity of strains near the fixed-end container boundaries and a higher level of energy trapped inside the model. Furthermore, higher spectral accelerations were captured in tests with

[1] **Corresponding author:** Associate Professor, Geotechnical Engineering Research Center, International Institute of Earthquake Engineering and Seismology (IIEES), No. 21, Arghavan St., North Dibajee, Farmanieh, Tehran, Iran, P.O. Box: 19395-3913, e-mail: yjafarianm@iiees.ac.ir

[2] Research Assistant, Geotechnical Engineering Research Center, International Institute of Earthquake Engineering and Seismology (IIEES), No. 21, Arghavan St., North Dibajee, Farmanieh, Tehran, Iran, P.O. Box: 19395-3913, e-mail: p.esmaeilpour@iiees.ac.ir
Board of directors, Iranian Earthquake Engineering Association (IEEA), Tehran, Iran.

[3] Graduated Student, Geotechnical Engineering Research Center, International Institute of Earthquake Engineering and Seismology (IIEES), No. 21, Arghavan St., North Dibajee, Farmanieh, Tehran, Iran, P.O. Box: 19395-3913, e-mail: saeed.shojaeemehr@iiees.ac.ir

[4] Graduated Student, Geotechnical Engineering Research Center, International Institute of Earthquake Engineering and Seismology (IIEES), No. 21, Arghavan St., North Dibajee, Farmanieh, Tehran, Iran, P.O. Box: 19395-3913, e-mail: hamed.taghavizade@iiees.ac.ir

[5] Graduated Student, Department of Civil Engineering, Semnan University, Central Administration of Semnan University, Campus 1, Semnan, Iran, P.O. Box: 35131-19111, e-mail: sadraroohi@yahoo.com

[6] Professor and Department Chair, Department of Structural Engineering, University of California San Diego, 9500 Gilman Dr., La Jolla, CA, 92093-0085, USA, e-mail: mccartney@ucsd.edu

fixed-end boundary conditions compared to those with flexible boundary conditions. Scaling issues associated with 1g shaking table testing were also discussed.

Keywords: Laminar shear container; Boundary condition; Shallow foundation; 1g shaking table; Saturated loose sand

Introduction

Considerable economic losses and casualties were reported in past earthquakes when the settlement, tilting, or bearing capacity failure of shallow foundations resulted in major damages to overlying super-structures (Tokimatsu et al. 1994; Yoshida et al. 2001; Bird et al. 2004; Bray and Dashti 2014; Bray and Lique 2017; Franke et al. 2019). Liquefiable soil layers may affect the seismic response of shallow foundations significantly, as shear stiffness and strength degradation of the soil may lead to bearing capacity failure or lateral spreading, while post-liquefaction drainage may result in excessive settlements and tilting of foundations. Examples of large earthquakes where shallow foundation issues were observed include the 1964 Niigata (Yoshimi and Tokimatsu 1977), the 1999 Kocaeli (Acacio et al. 2001; Bray et al. 2000), the 2007 Peru (Taucer et al. 2009), the 2010 Chile (Bertalot et al. 2013), the 2011 Tohoku (Tokimatsu et al. 2012), the 2011 Christchurch (Bray et al. 2014), and the 2016 Kumamoto earthquakes (Tokimatsu et al. 2019).

Various approaches have been employed to evaluate the seismic behavior of shallow foundations, such as analytical and numerical modeling, reduced-scale or full-scale physical model testing at 1g, small-scale physical model testing at an elevated acceleration field (Ng) in a geotechnical centrifuge, and the empirical models originated from the field reconnaissance reports of actual earthquakes. Of these methods, reduced-scale physical modeling experiments at 1g and in a geotechnical centrifuge at Ng can be beneficial to gain insight into seismic problems as they permit parametric evaluation with controlled specimen preparation and testing, and can be densely instrumented. These experimental approaches also permit straightforward interpretation of ground amplification and soil-structure interaction (SSI) problems, and in the right conditions may result in realistic variations of the co- and post-seismic excess pore water pressure (EPWP) and consideration of soil nonlinearity.

Numerical studies have been performed to evaluate the mechanisms and understand key parameters controlling the shear-induced settlement of structures resting on shallow foundation due to soil liquefaction (Pane et al. 2016; Macedo and Bray 2018; Karimi et al. 2018; Forcellini 2019). Furthermore, probabilistic methods have been used to assess liquefaction potential in addition to liquefaction-induced settlement of shallow foundations (e.g., Jafarian et al. 2013; Shahnazari et al. 2016; Bullock et al. 2018). Field observations and reconnaissance studies were also employed to evaluate case histories and key factors controlling the settlement and tilting of existing structures based on observed damages in recent earthquakes (Yoshimi and Tokimatsu 1977; Acacio et al. 2001; Bray et al. 2000; Bertalot et al. 2013; Bray et al. 2014; Tokimatsu et al. 2012; Tokimatsu et al. 2019). Moreover, numerous experimental studies have investigated different aspects of seismic behavior of shallow foundation on dry or saturated condition using physical models in both 1g shaking table and Ng centrifuge tests (Liu and Dobry 1997; Adalier et al. 2003; Dashti et al. 2010a; Dashti et al. 2010b; Hayden et al. 2014; Jafarian et al. 2017; Mehrzad et al. 2018; García-Torres and Madabhushi 2019; Jafarian et al. 2020).

A majority of previous physical and numerical modeling studies concentrated on understanding the mechanisms and key parameters governing the settlement and tilting of shallow founded-structures during earthquakes. However, the effects of lateral boundary condition on the seismic performance of the shallow foundations have not been systematically investigated in direct comparisons. Only a few studies are available in the literature involved investigation of boundary condition effects on soil responses in free-field conditions (Whitman and Lambe 1986; Lee et al. 2012), slopes (Hung et al. 2018), or for a shallow foundation on dry sand (Pozo et al. 2016). No previous research is available where the effects of boundary conditions in terms of flexible and fixed-end on response was compared for different soil-structure interaction conditions (e.g., free field conditions, shallow foundation on saturated sand, shallow foundation beneath a single degree of freedom (SDOF) super-structure on saturated sand).

Whitman and Lambe (1986) compared the performance of containers with different boundary conditions when modeling a sand layer in centrifuge base shaking experiments. They compared the response of a soil layer in a rigid container with the same soil condition in a container consist of a number of stacked-ring devices with different aspect ratios to evaluate geometrical limitations and model performance. They concluded that even distant walls can affect the results when liquefaction occurs. Fiegel et al. (1994) compared the performance of the Caltech LSB container, the Cambridge equivalent shear beam (ESB) container, and a rigid container with that of a hinged-plate container (HPC) in shaking table tests in the geotechnical centrifuge at UC Davis. They found that LSB containers have smaller values of acceleration amplification ratio and higher natural frequency compared to the other containers and this could lead to lower system stiffness. This is essential if the design goal for the container is for the soil movement to govern the system deformation.

Lee et al. (2012) examined boundary effects of an LSB container using dry and saturated sand models. They found that the main frequencies, acceleration amplitude phase lags, and the profiles of the obtained root mean square accelerations remained intact if the distance of instruments from the moving end walls were more than one-twentieth of longitudinal dimension of the model. Moreover, they observed that discrepancies between the measured EPWP at the model center and at a distance of one-fourth of the long side of the model from the lateral boundaries are negligible. Pozo et al. (2016) focused on the assessment of soft lateral boundary effects on a shallow foundation in terms of pre- and post-peak load-displacement responses using the particle image velocimetry (PIV) method. They observed the strain development at stiff and softer lateral boundaries and identified a relationship between these observations and the mechanical behavior of the shallow foundation. Hung et al. (2018) investigated the effects of fixed and flexible boundary conditions on the response of slope in liquefiable site and showed that the slope experienced different accelerations in the fixed and flexible boundary conditions. Ghayoomi et al. (2013, 2014) evaluated the response of an acrylic flexible shear beam (FSB) container that permitted visual observation of buried structures during shaking table testing in the centrifuge while still maintaining plane strain conditions and hydraulically-sealed conditions.

This paper first presents the design and construction of a new light-weight, acrylic, single-axis LSB for use in 1g shaking table testing. Dynamic performance of the container was then assessed through a series of 1g shaking table tests on loose sand layers in both dry and saturated conditions. For the main testing program, three series of 1g shaking table tests were then performed to evaluate the boundary effects of the container on the distributions of acceleration, displacement, and EPWPs in saturated, loose sand layers in (1) free-field condition, (2) with a shallow foundation, and (3) with a shallow foundation supporting a SDOF super-structure. Considering the results of the tests on a saturated, free-field sand layer as a reference, the impacts of including a solitary shallow foundation resting on the sand surface, and a shallow foundation supporting SDOF super-structure were investigated.

Container boundary conditions

In both 1g and Ng shaking table experiments on soil layers, a container is needed to retain both the soil and pore fluids. To properly model one-dimensional (1D) wave propagation in a finite soil stratum in a shaking table experiment, the following criteria for container designs should be satisfied: (1) the horizontal cross-section of the container should remain constant during shaking to maintain plane strain conditions (zero lateral strain); (2) the walls of the container in the shaking direction should not impede the movement of the soil in response to basal shaking; (3) the mass of the container should be as low as possible to lessen the dynamic inertial forces at the boundaries, and approximately zero stiffness for horizontal shearing to make sure the soil governs the system movement; and (4) the end walls of the container must be roughened so that complementary shear stresses can be developed that match existing shear stresses on the container base (Whitman and Lambe 1986; Zeng and Schofield 1996).

One of the critical issues in physical modeling of geotechnical problems is to reproduce, as close as possible, lateral boundary conditions representative of those in a field setting to minimize undesirable effects on test results. Lateral boundary conditions can have a significant impact on the model response in physical modeling experiments and may alter the dynamic behavior of a soil system lead to preventing correct simulation of free-field response (Lee et al. 2012). Hence, considering these effects in shaking table tests in both 1g and Ng is crucial when analyzing model behavior and interpreting the results.

In the last four decades, several efforts have been made by different researchers to design and develop different types of containers, including: (1) rigid or fixed-end containers (Fishman et al. 1995), (2) rigid containers with flexible boundaries (Pozo et al. 2016), (3) hinged-plate containers (Whitman and Lambe 1986), (4) flexible shear beam (FSB) containers (Ghayoomi et al. 2013 and 2014), (5) equivalent shear beam containers (Zeng and Schofield 1996), (6) laminar shear beam (LSB) containers (Hushmand et al. 1988; Turan et al. 2009), and (7) active boundary containers (Takahashi et al. 2001). Both 1g and Ng shaking table tests have been conducted using these types of containers to understand their key properties and performance in modeling 1D wave propagation in soil column. Among all developed containers, LSB containers are the most popular due to their accuracy in modeling realistic site (Li et al. 2020). An LSB comprises a stack of laminates (or frames) supported individually by bearings that can be mounted on a shaking table and deform in the direction of motion to mimic the free-field displacement of a soil layer during basal shaking. The bearings allow relative displacement between the frames with minimal friction and facilitate relatively free movement of the soil layers similar to the in-situ conditions. Table 1 summarized laminar shear containers employed in previous studies by different researchers.

Rigid or fixed-end containers were the first container type used in physical modeling experiments to determine the seismic bearing capacity of shallow footings (Okamoto 1956).

Rigid containers are unable to replicate the realistic free-field seismic response of soil layer overlaying a rigid rock mainly due to three important issues (see Fig. 1): (1) Strain dissimilarities at the boundaries due to fixed end walls that restrict soil deformation (Zeng and Schofield 1996), (2) Lack of complementary shear stress near the smooth end walls (Lee et al. 2012), and (3) generation of P-waves due to interaction between the soil and fixed-walls which find no way out to the infinite half-space, effectively trapping them inside the model owing to the fixed-end artificial boundaries (Lee et al. 2012).

One of the crucial issues in performance of the model containers is their size. Effects of container size on the soil response in laminar shear containers have not been investigated to date and no related research in the literature practically examined this issue. An intuitive understanding would be that the larger the model is, the more precise the model response will be (Zhang et al. 2008). For instance, the full-scale prototype (N=1) could be considered as the ideal model. However, bigger container size required stronger laminates profile resulting in higher box to soil mass ratio that could affects the soil response due to augmented inertial forced. Moreover, increased container mass could have undesirable effect on bearing performance in providing freely movement of adjacent laminates.

In rigid or fixed-end containers, change in size could have major impacts on soil responses, leading to unrealistic/misleading results. A rigid container has to be large enough to correctly replicate the free-field site response. Fishman et al. (1995) reported that the free-field soil response may not be realized in the rigid containers for distances up to 1.5H to 2H from the fixed end walls, where H is the container height. It means the rigid container length should be 4H to reproduce free-field condition over the central portion of the model.

Experimental Setup

Laminar shear container

The laminar shear container at International Institute of Earthquake Engineering and Seismology (IIEES) was designed for 1g shaking table to perform seismic modeling of soil layers subjected to 1D earthquake-like input motions at the model base. It was designed to test saturated or dry soil models and allow developing of complementary stresses related to 1D wave propagation. Complimentary shear stresses are mobilized at the boundaries in the direction of shear via roughened end walls. Fig. 2 shows views of the fabricated LSB on the shaking table in addition to laminate plan and sections of longitudinal and transverse I-beams.

Based on extensive review of available LSB containers in the literature summarized in Table 1, the authors decided to specify the container inner length to height ratio (L/H) to be 1.4 and the inner length to width ratio (L/W) to be 1.5. An optimization analysis was employed to calculate the optimal values of length, width, and thickness of longitudinal and transverse beams. As a result, L=500 mm was chosen for the container outer length. By choosing the outer length of the container (i.e. L=500 mm), longitudinal and transverse beams were then designed and the internal dimensions of the LSB was eventually obtained: 364.8 mm in length, 242.8 mm in width, and 263 mm in height (L×W×H). Allowable stress design (ASD) method was used to design all structural elements to resist maximum estimated forces acting on each element in seismic condition. Furthermore, additional estimated loads were considered in the container design calculation so that the container height could be extended to 500 mm if necessary.

The container consists of 18 light-weight acrylic laminates arranged in a stack to provide flexible lateral boundaries. Acrylic was chosen because: (1) it is lightweight so that the inertial effects of the container on soil layer movements could be minimum due to low box to soil mass ratio; (2) the whole system movement is visible due to material transparency; and (3) ease of machining and assembly/disassembly of acrylic material which facilitate convenient maintenance. The laminates are made of I-beams, with 67.6 mm in depth for the transverse beam and 45.8 mm for the longitudinal beam. The height of each individual beam in both transverse and longitudinal beam laminates is 11 mm.

The base laminate was firmly fastened to the shaking table platform via bolts. The laminates components consist of stoppers, rollers, and plastic holder for rollers. The 5×8 mm cubic stoppers were also implemented in the transverse beams of the laminates in order to limit the relative displacement between the layers in longitudinal direction. Since the stoppers are embedded within the layer interfaces, there is no need of external mount to limit the deformation for possible container instability. In order to facilitate freely relative movement of the frames and decrease friction between them and to obtain a uniform weight distribution, 40 acrylic rollers (with 10 mm diameter) were interlaid between each laminate. Each laminate can slide laterally up to 4 mm relative to the adjacent laminate in the longitudinal direction. The maximum cumulative lateral displacement of the LSB top layer is 68 mm with a total achievable shear strain of about 26%. This large displacement is provided to accommodate large deformation phenomena like liquefaction-induced lateral spreading. The approximate friction coefficient of each frame during sliding is 0.01 and the frame-to-soil mass ratio is 0.24.

A 0.44 mm-thick latex membrane bag was fabricated to fit within the box to retain water and soil grains inside the container. The total mass of the empty LSB is 15.6 kg and when filled with saturated sand having a total density of 1966 kg/m^3 its total mass is 62.2 kg. To prevent contact interference between laminates during container shaking and to minimize volumetric strains due to membrane bulging, 4 mm vertical gaps are provided between each adjacent laminate. The IIEES laminar shear container properties are summarized in Table 2.

Shaking Table

The IIEES 1g shaking table used for the experiments acts in a single direction and consists of a 1.4 m × 1.2 m platform that is driven by hydraulic actuators controlled by a digital control unit. The table can simulate realistic earthquake motions as well as single- or multi-stage input motions including harmonic spectrum motions, band-limited motions, impulse load motions, and white noise spectrum motions. The shaking table has a frequency output range of 1 to 400 Hz, a maximum stroke of 35 mm in the excitation direction, and a 20 kN base shear capacity.

Similitude laws for 1g shaking table testing

Because of the size of the container, only reduced-scale soil-structure interaction experiments may be performed. Accordingly, similitude laws should be employed to extrapolate the behavior from the shaking table tests to full-scale systems (prototype scale). Different sets of similitude laws for reduced scale models at 1g have been established in the literature (Kagawa 1978; Kokusho and Iwatate 1979; Iai 1989; Maymand 1998). Of these, Iai (1989) derived a set of similitude relations particularly for saturated sand in 1g shaking table tests in which most key parameters were taken into consideration to approximately reproduce field condition. Iai (1989) also examined the applicability of the derived similitude relations through available tests results and reported that the similitude will give a good approximation on the behavior of the prototype. Nevertheless, the low self-weight stress level at 1g gravitational field inevitably affect the stress-strain and seismic response of the sand layer in physical model tests. Specifically, excess pore water pressure (EPWP) generation and dilatancy behavior in sands are dictated by combined effects of density and effective stress level. To overcome this difficulty, Toyota et al. (2004) suggested procedures such as using a modified grain size distribution, lower relative density, higher frequency of loading, and application of more loading cycles in the 1g shaking table tests to retain similitude with field-scale test results. Vargas-Monge (1998) recommended use of a lessened relative density in the model compared with that of the prototype using concept of brittleness index. The relative density of the soil layer in the model can be determined by maintaining the brittleness index constant between the prototype and the model.

In order to evaluate the applicability of the employed scaling laws in physical model tests, numerous studies have compared shaking table tests at 1g and Ng to identify appropriate scaling factors relating the corresponding results in both experiments (Gibson and Scott 1995; Hayashi et al. 1997). In these studies, satisfactory agreement was observed between the results of 1g shaking table tests and those of Ng centrifuge tests. Also, they all indicate that if the shaking table tests are being performed carefully, application of proper scaling factors plays an important role to achieve reliable results. Accordingly, 1g shaking table tests may be useful in validating future centrifuge modeling studies.

In the current study, the scale factors derived by Iai (1989) were employed to relate reduced-scale model and full-scale prototype parameters in the 1g shaking table tests which are summarizes in Table 3 with adopted scaling factor of N=16.7. To compensate for the deficiency of the lower confining stress in the current 1g model tests, the sand relative density in the model test ($D_r = 30\%$) was chosen to be lower than that representative of the prototype ($D_r = 57\%$). In other words, dilatancy of the sand is kept constant in the model and prototype by adjusting the stress-density state, decreasing the relative density of the model sand to compensate for the increased dilatancy produced by the smaller effective stress in the model. Further, higher loading frequency (i.e. 10 Hz) and more loading cycles (i.e. 80 cycles) were applied as a base input motion to retrieve for low self-weight stresses in the current experiments.

Soil properties

Babolsar sand was employed in the shaking table tests, which classifies as poorly graded sand (SP) according to USCS classification system. The sand has zero fines contents (FC=0%) and a mean particle size of $D_{50} = 0.15$ mm. The minimum and maximum void ratios of the Babolsar sand are $e_{min} = 0.632$ and $e_{max} = 0.868$, respectively. The specific gravity of solids is $G_s = 2.74$. The grain size distribution is shown in Fig. 3. Babolsar sand has been used in recent experimental studies that have reported other geotechnical properties of this material (Jafarian et al. 2016; Jafarian et al. 2019).

Input motion

The base input motion for all experiments consisted of 80 sinusoidal wave cycles with a 0.3g acceleration amplitude at 10 Hz frequency, lasting for eight seconds as shown in Fig. 4. The long loading duration is to compensate for the lower confining stresses in the reduced-scale 1g model tests and to simulate a worst-case scenario of soil subsidence as well as tilting and/or settlements of structure model during shaking. The sinusoidal wave was chosen for the input excitation mainly to permit simple interpretation of results owing to the inherent symmetry of the constant magnitude sine-type seismic excitations. The acceleration amplitude of 0.3g was selected to ensure the triggering of liquefaction during shaking.

Model preparation

Soil layer preparation

Dry sand was placed by air pluviation within the LSB container to form uniform layers having a relative density of $D_r = 30\%$ (dry density of 1966 kg/m3) in model scale until the box is filled. The drop height used in pluviation was varied using trial and error to reach consistent relative densities. During pluviation, sensors were embedded at the designated locations as shown in instrumentation layout. For the tests performed on water-saturated sand layers, after injecting CO_2 into the model to expel pore air, de-aired water was then flushed slowly upward through the sand layer from the base until the water table reached 5 mm above the soil surface. After approximately two hours, surplus water on the soil surface was removed using a sponge. Then, the water level was set to be at the soil surface. From measuring the amount of water flushed into the model and dividing by the required water needed for full saturation, the degree of saturation was calculated. The calculated degree of saturation was above 90% for all tests. For the second and third test series, the shallow foundation (with or without a superstructure) was then placed atop of the soil surface. Immediately after the installation of shallow foundation, vertical displacements were monitored through an image processing technique during a consolidation phase prior to the shaking onset. Initial captured settlements values were less than 0.9 mm for all tests which was deemed negligible compared to the permanent settlements (17~33 mm) measured during the shaking phase.

In reduced-scale 1g shaking table tests where confining stress levels are low, it is essential to characterize proper stress-strain relation in agreement with the prototype especially for considering dense sand dilatancy behavior. The loose sands dilatant behavior at low stress levels in a 1g shaking table tests generally simulate the denser sand behavior in prototype. Vargas-Monge (1998) carried out a series of element testing under constant volume condition and tried to lessen the effects of stress levels by changing the soil relative density and then developed the softening extent calculated by the brittleness index (I_B) which previously suggested by Bishop et al. (1971). The relative density can be determined by maintaining the undrained brittleness index constant between the prototype and the model in the expression proposed in Eq. (1):

$$\frac{e_m}{e_p} = 1 + \frac{0.052}{e_p} \log_{10} N \tag{1}$$

where e_m and e_p are model and prototype void ratios, respectively, while the scale factor, N, is equal to 16.7 in the current study. To compensate for the lower confining stress in the current 1g model tests, the sand relative density of the model was chosen to be lower than that representative of the prototype. The loosest achievable state of Babolsar dry sand in the container was $D_r = 30\%$ (or void ratio of $e_m = 0.797$) which is equivalent to $D_r = 57\%$ (or void ratio of $e_p = 0.734$) in the prototype scale based on adopted scaling factor (N = 16.7). In other words, a prototype made of Babolsar sand with a relative density lower than $D_r = 57\%$ is unlikely to be modeled in the constructed LSB with dry deposition procedure. Hence, this void ratio limitation requires first determining the model relative density prior to model any specific prototype. By employing Eq. (1) and assuming a model void ratio of 0.797 ($D_r = 30\%$), the prototype void ratio was calculated to be 0.734 ($D_r = 30\%$) using the adopted scaling factor (N = 16.7).

Overview of testing program

The overall testing program conducted in this study are as follows:

- *Preliminary tests:* performance evaluation of the LSB container; (1) free-field test on dry sand (PFFD), (2) free-field test on saturated sand (PFFS).
- *Main tests*: investigating of boundary condition effects on model response: (1) first series: free-field condition on saturated sand with flexible boundary (FFL) and fixed-end boundary (FFR), (2) second series: shallow foundation on saturated sand with flexible boundary (SFL) and fixed-end boundary (SFR), (3) SDOF super-structure on shallow foundation with flexible boundary (SSFL) and fixed-end boundary (SSFR).

Details of the testing program and loading characteristics are summarized in Table 4.

In preliminary tests, two 1g shaking table tests (PFFD and PFFS) were carried out on loose sand layers ($D_r = 30\%$) in both dry and saturated conditions to investigate the performance of the LSB in modeling 1D vertical wave propagation in finite soil column. Each model was shaken longitudinally under a sinusoidal input with an acceleration amplitude of 0.3g and frequency of 10Hz for 8 seconds as shown in Fig. 4.

For the main testing program, three series of 1g shaking table tests were carried out to explore the effects of container boundary conditions on saturated loose sand layers ($D_r = 30\%$). Specifically, the testing program was designed to study effects on EPWP generation and liquefaction-induced settlement of shallow foundations and free-field ground. Each series consists of two similar tests that differ only in the lateral displacement boundary condition. The first test of each series was conducted with a flexible boundary where the container layers can move freely with soil and the second test was conducted with a rigid, fixed-end condition where the container layers are restrained from moving.

In the first testing series (FFL and FFR), the free-field responses of saturated sand layers were evaluated for both fixed-end and flexible boundary conditions. In the second testing series (SFL and SFR), a rigid steel block was positioned on the sand layer surface as an equivalent shallow foundation. In these tests, the main objective was to assess the container boundary effects on the soil response in terms of EPWP generation and surface settlement. For the third testing series (SSFL and SSFR), an SDOF was placed atop a thinner shallow foundation to examine the effects of the container on SSI mechanisms under the same contact stress as in the tests in the second testing series.

Shallow foundation and SDOF model

In practice, shallow foundations are generally made of reinforced concrete. However, in physical modeling experiments, the shallow foundation models are usually made of material with higher density such as steel (with $\rho = 7800\ \mathrm{kg/m^3}$) or brass (with $\rho = 8700\ \mathrm{kg/m^3}$) to provide required contact pressure representing an actual building in prototype scale according to similitude laws. Due to the dimension limitation in reduced-scale physical modeling tests, concrete with lower density (i.e. $\rho = 2500\ \mathrm{kg/m^3}$) was not an appropriate option for shallow foundation models. Target contact pressure of shallow foundation and/or super-structure mass cannot be achieved by using low-density material such as concrete, so steel was used for the footings.

In the second testing series, the shallow foundation was a rigid block of ST37 steel having a length of 240 mm (4 m in prototype scale) and a width of 60 mm (1 m in prototype scale) shown in Fig. 5 (a). The shallow foundation stretches across the width of the box; thus, plane strain condition can be assumed in these tests because out-of-plane deformation of underlying soil is restricted by the container walls. The shallow foundation has a total contact pressure of 39.9 kPa which represents the prototype-scale surcharge stress representative of a three-story building assuming that the foundation mass corresponds to a single-story mass.

In the third testing series, an SDOF super-structure was created by attaching a rigid steel cylinder to a thinner shallow foundation so that the contact stress would be approximately the same as the shallow foundation in the second testing series (see Fig. 5 (b)). The stiffness and mass of the SDOF super-structure were calculated to represent an equivalent three-story building. The structure models of the shallow foundation and SDOF on shallow foundation are shown in Fig 5. In both second and third testing series, the bottom face of the shallow foundation which was in direct contact with soil was roughened to provide friction between the soil and the shallow foundation model. The mechanical and geometrical properties of the shallow foundation and the SDOF resting on a shallow foundation model are summarized in Table 5.

The shallow foundation structural models were positioned on the soil surface without any embedment in both second and third test series. By embedding the shallow foundation into the soil layer, ground disturbance will occur inevitably which could seriously affect the test results in small-scale 1g shaking table tests. Thus, the current model preparation procedure was configured to minimize soil disturbance by placing the shallow foundation atop of soil surface in order to achieve uniform homogeneous sand layer with relative density of $D_r = 30\%$ in model scale. Undesirable effects of sample disturbance on results could be more pronounced when the model is made of loose sand that could be easily disturbed (Kumar et al. 2020). Moreover, the scaled embedment depth in the model tests is relatively small and it might be impractical in model test preparation.

Instrumentation

Detailed instrumentation layouts for the tests in the experimental program are shown in Fig. 6. The sensors include five uniaxial accelerometers, two pore pressure transducers, and a linear potentiometer placed on the soil or foundation surface to quantify the settlements during and after shaking. Two of the accelerometers (A3 and A2) were installed in a vertical array in the center of the model at various depths and the other one was placed on the base layer of the container for measuring the actual input motion (A1). The last accelerometer (A4) was installed on the soil surface at the right-end side of the container for all tests. The right-end accelerometer was installed 30 mm away from the end boundary (approximately one-tenth of the model length) to capture the near-boundary acceleration response.

In the second testing series, an accelerometer was mounted on the shallow foundation while in the third testing series an additional accelerometer was mounted on top of the SDOF super-structure. In all testing series, two pore pressure sensors were embedded in a vertical array at the mid-height and base of the sand layer. In the first testing series, the extension rod of the potentiometer was glued to a thin acrylic plate placed on the soil surface horizontally. The acrylic material for the plate was selected because its density is approximately equal to the density of the liquefied soil whereas the plate settles with the soil surface. Image processing was also used to capture horizontal displacements of the container layers and to track the foundation and SDOF super-structure displacements. Pore pressure at various depths, acceleration time histories, surface settlement, and layers displacement were recorded simultaneously during each test. The measured data are presented in model scale units unless otherwise noted.

Results and discussion

Assessment of the LSB performance

To investigate the performance of the laminar shear container in modeling 1D vertical wave propagation in the finite soil column, preliminary shaking table tests were performed on loose sand layers in both dry and saturated conditions. In these tests (i.e., PFFD and PFFS), the soil layers were subjected to harmonic motion shown in Fig. 4. The sand response at the surface right-end and surface center of the container in both dry and saturated conditions are compared in Fig. 7 in terms of acceleration time history and spectral acceleration. The results show that the maximum difference between the right-end and center acceleration time histories does not exceed 7% which indicates that the boundary effect on recorded right-end acceleration is negligible and the container is flexible enough to properly model 1D soil column. Similar trend is especially visible in the spectral acceleration response of the surface center and surface right-end in both dry and saturated conditions (Fig. 7 (e) and (f)). It can be inferred that the container provides low boundary constraints during shaking of the model, while still having the sufficient rigidity to keep nearly at-rest horizontal stresses and plane-strain boundary conditions during shaking.

Boundary effect on the settlement and EPWP

The effects of container boundary conditions on surface settlements and EPWP time histories during and after shaking at various depths for the three testing series are demonstrated in Fig. 8. The highlighted sections in the graphs reflect the base input shaking time span and the dashed lines in the EPWP graphs reflect the onset of liquefaction ($r_u = 1$). The ratio of pore water pressure, r_u was calculated as the attained generated pore water pressure, Δu, divided by the overburden effective vertical stress at the corresponding elevation, σ'_{v_0} as follows:

$$r_u = \frac{\Delta u}{\sigma'_{v_0}} \tag{2}$$

It is noting that the surface surcharge for the second and third test series was taken into account in the calculation of the effective overburden stress in Eq. (2). As shown in Fig. 8, the surface settlements in the tests with fixed-end boundary condition (FFR, SFR, and SSFR) are more pronounced in comparison to the flexible ones (FFL, SFL, and SSFL) as expected due to higher energy level trapped inside the model (see Fig. 1). The maximum amount of permanent settlement is observed in shallow foundation case with fixed-end boundary condition with 33 mm in model scale which has increased by 112% compared to the corresponding flexible condition (Fig. 8 (b)), while the increase of settlement for free-field and SDOF super-structure conditions are 115% and 58%, respectively (Fig. 8 (a) and (c)). Settlement began to occur immediately from the first couple of cycles and continued with higher rate for fixed-end conditions. Settlement of the models continued to take place with very low rate, even after the base shaking finished especially when super-structure exists, until the termination of reconsolidation in the superior layers, but for better resolution only the first thirty seconds are shown in the graphs. However, the cumulative amount of the post-seismic settlement is negligible compared to the co-seismic settlements.

In the free-field tests (FFL and FFR), the transient EPWP rapidly increased from zero to a constant level for the flexible case (FFL) and the model was thoroughly liquefied during the first cycles of shaking at mid-height and base of the soil layer (see Fig. 8 (a)). Similar trend was observed for the FFR test; however, the maximum EPWP never reached the liquefaction limit in both elevations (mid-height and model base). Once shaking ceased, pore water pressure dissipation began in both fixed-end and flexible models with a little delay in flexible condition. This delay in EPWP dissipation is attributed to upward migration of pore water and solidification front after the end of shaking which begins at the base layer followed by delayed pore pressure dissipation in the above layers. In post-shaking time, the dissipation rate was noticeably higher in the flexible condition compared to the fixed-end condition especially in the model base. Further, higher fluctuations in EPWPs were observed in the fixed-end condition due to the existence of unwanted superfluous waves.

In the second series of tests (SFR and SFL), fully liquefaction was not observed beneath the foundation. The amount of EPWP in the soil layer beneath the shallow foundation was slightly higher than those in free-field test but the peak of EPWP was considerably far from the liquefaction limit ($r_u = 1$). Similar to the second test series, for the shallow foundation with an overlying SDOF (i.e. SSFL and SSFR tests), the amount of EPWP in the soil layer beneath the structure was higher than those in free-field. In fact, only partial liquefaction occurred in the soil immediately beneath the foundation ($r_u < 1$). Dissipation rate in the whole soil column was higher for flexible condition.

Boundary effect on the acceleration response

The input acceleration introduced at the model base propagates in vertical direction along the soil stratum and may be attenuated or amplified depending on the characteristics of the input excitation and the dynamic properties of the soil. Acceleration time histories for all test series are shown in Fig. 9. The dashed lines in the acceleration graphs reflect the input motion acceleration amplitude (0.3g). Comparison of the time histories indicates that there are discrepancies between the acceleration time histories recorded at various locations inside the model in both flexible and fixed-end boundary conditions in free-field, shallow foundation, and SDOF super-structure on a shallow foundation. During the initial cycles of shaking, acceleration responses were fairly identical at the various depths of both flexible and fixed-end conditions in all tests, since soil stiffness degradation is not high enough during the initial cycles of shaking.

In the free-field tests (FFL and FFR), after the first stages of loading, the acceleration response was attenuated for the flexible case at the mid-height and then slightly amplified in higher level. The former phenomenon indicates on a shear localization within the sand somewhere between mid-height and bottom of the model. However, this trend in fixed-end condition was not analogous after soil degradation commenced; the acceleration time history at mid-height is almost identical to the base input and from the mid-height to the surface, a decay in acceleration response is visible (see Fig. 9 (a)). This difference is likely due to P-waves generated by reflections from fixed-end walls during shaking. However, the values of peak acceleration increased while propagation of the wave from the base to the surface.

In the tests with shallow foundation (SFL and SFR), the values of peak acceleration increased as the input wave traveled from the mid-height to the soil surface. At shallower depths of the fix-end container, the sand response is more affected by the softening of underlying sand and caused more noticeable acceleration changes with time. In contrast, in flexible condition, a relatively smooth acceleration response was captured.

For the shallow foundation tests with overlying SDOF super-structure (SSFL and SSFR), analogous trend was captured indicating an increase of the peak acceleration values at the beginning of loading cycles from the mid-height to the surface for the rigid condition. Nevertheless, the accelerometer installed on top of the foundation measured different responses for the rigid case compared to the corresponding shallow foundation case probably due to SSI effects. The acceleration responses at the top of foundation were not amplified during the first cycles of shaking. For the rest of loading cycles, attenuation in acceleration responses are obvious which may be attributed to softened subsoil layer. For the flexible boundary condition case, the peak acceleration values at the beginning of the loading decreased as the input wave propagated along the soil layer from base to soil surface. After the initial cycles of shaking, increases in soil softening resulted in a higher damping ratio within the soil layer which in turn lead to significant phase lag between input and measured acceleration in all elevations. This could explain the acceleration necking after the early loading cycles in all tests with flexible boundary condition.

Similar to the recorded acceleration time histories, the spectral acceleration responses derived from the accelerometers with 5% damping ratio are shown in Fig. 10 at various locations for free-field, shallow foundation on soil surface, and SDOF super-structure on shallow foundation during the shaking. Higher spectral acceleration amplitude for the fixed-end condition is observed especially near the input motion frequency (T=0.1s) for all the cases most likely because of response amplification in fixed-end condition due to higher energy level. The evident lower acceleration amplitudes shown in Fig. 10 for the flexible conditions are mainly due to freely movement of the container layers. The slight shift of peak spectral acceleration to the right for the flexible condition curve indicates that the flexible container stiffness is lower compared to the fixed-end boundary condition.

Results of image processing analysis of layers

Visualizing displacement of the container layers could be very helpful for better understanding of container performance and system response to base input while shaking. Image processing technique was used for capturing horizontal displacement of container layers during shaking for all test series. For this purpose, as shown in Fig. 11, two synchronized cameras were used to simultaneously capture the displacement of soil surface and points on structure in addition to horizontal movements of container layers. Fig. 12 shows the results of the image process analysis of odd layers from the base layer to the 17th layer for the flexible tests in comparison with the base (or rigid) displacement input.

In the first couple of loading cycles, displacement of layers almost matches the base input, but immediately after, maximum layer displacements decayed to an approximately constant value. Displacement of the 3rd layer was almost identical to the base input in all three testing series. However, the peak values of displacement diminished from the highest value at the base (1st layer) to the lowest value near the sand surface (15th layer). The remarkable difference between measured displacement at layer 15 and layer 17 can be inferred as a shear localization near the 15th layer. Nevertheless, more irregularity can be seen in displacement time history for the second and third test series near soil surface probably due to super-structure and SSI effects on responses.

At shallower depths, where soil responses are affected by the softened deeper layer, displacement changes with time are more noticeable. Hence, deviation in maximum displacement response of layers is considerably larger particularly at shallower depth for shallow foundation and SDOF on shallow foundation.

The results of the image process analysis of layers displacement from the base layer to the top layer (18th) are plotted in Fig. 13 between t=1s and t=1.6s of the shaking time (a, c, and e) with 0.1 second time steps and t=2s to t=8s (b, d, and f) with the corresponding pore pressure build-up ratio (r_u) for free-field condition, shallow foundation, and shallow foundation with a SDOF super-structure. In the free-field condition, after t=1.2s (Fig. 13 (a)), the displacement of the 10th layer decrease significantly and relative displacement of the above layers declined to zero which can be inferred that shear localization has taken place somewhere near 10th layer due to pore pressure build-up. This was first apparent in Fig. 9 (a) for the acceleration response near mid-height in free-field condition. Significant reduction in acceleration responses at the mid-height in Fig. 9 (a) could be caused by formation of shear localization somewhere near mid-height preventing waves from traveling upward along the soil layer. Thus, the above layers (11th to 16th) move like a rigid body without any shear deformation until the last two layers (17th and 18th layers) that are close to the soil surface where the strain non-uniformity is considerable. However, for the rest of the shaking time (t=2s to t=8s), layers displacements decrease significantly and barely surpassed 0.6 mm. This trend is especially seen in Fig. 12 following the first couple of cycles when the pore pressure ratio reaches its maximum value.

In the cases with shallow foundation (2nd and 3rd test series), the layers displacement for the time span of 2s<t<8s are larger in comparison with the free-field condition. This may refer to incomplete liquefaction mainly because of the existence of shallow foundation on the soil surface. The additional surcharge imposed by placement of the shallow foundation leads to an increase in effective stress and confining pressure beneath the foundation which is a beneficial factor in minimizing EPWP build-up during shaking. At the same time, soil beneath and around the foundation tends to move laterally due to largely applied shear stress. This mechanism causes the soil to dilate, resulting in a reduced EPWP build-up and incomplete liquefaction ($r_u < 1$) in this region (Mehrzad et al. 2018).

In some recent experimental studies in both 1g shaking table and Ng centrifuge tests, lower or even negative EPWP beneath the foundations have been reported compared to free-field soil responses (Alam and Towhata 2008; Adalier et al. 2003). In another research, Karimi et al. (2015) showed that a reduction in excess pore pressure ratio (r_u) under the foundation is observed compared to the free-field condition, due to elevated confining pressure in the soil layer. However, this increased resistance to EPWP generation and liquefaction under the foundation was experimentally shown to depend on building's confining pressure, relative density of soil, and ground motion intensity. Sand with a higher relative density is more resistant to seismically-induced EPWP build-up and strength loss. Hence, complete liquefaction ($r_u = 1$) was observed in the free-field but not under the footing.

In the shallow foundation condition (Fig. 13 (c) and (d)), the 14th layer has the smallest displacement before t=1.6s, but remarkable decrease in recorded displacement of the 8th layer for the period of 2s<t<8s indicates two different localizations probably occurred in different times which the last one lead to different soil behavior between above and below the 8th layer. For the shallow foundation with an SDOF super-structure, shear localization occurred in the 13th layer and similar to the free-field conditions, the displacements in the uppermost layers were smaller. The same trend for the last two layers (17th and 18th layers) is also visible as the free-field condition.

Summary and conclusion

As preliminary tests, two 1g shaking table tests were performed to investigate the seismic performance of the newly constructed LSB on saturated and dry loose sand deposit in modeling the free-field condition. The container was designed in a way that can provide both flexible and fixed-end boundary conditions by adding elements to the moving end walls to restrain layers horizontal displacement. The results of preliminary tests confirm that the LSB permits free movement of dry and saturated loose sand layers. Besides, the container provides low boundary constraints during shaking of the model, while still having sufficient rigidity to keep nearly at-rest horizontal stresses and plane-strain boundary conditions during shaking. Then, three series of 1g shaking table tests were conducted as a main testing program to evaluate the impact of boundary conditions on the seismic response of saturated sand layers (1) in free-field conditions, (2) with a shallow foundation, and (3) with a shallow foundation supporting a single degree of freedom (SDOF) super-structure on saturated loose sand layers. Specifically, the effects of fixed-end and flexible boundary conditions on the excess pore water pressure (EPWP) build-up, surface settlement, and acceleration response were evaluated in direct comparisons for the main testing program.

According to the results of the main experiment program, the following conclusions can be drawn on the issue of container boundary condition effects in 1g shaking table tests conducted on saturated loose sand:

1) Surface settlements for sand layers with fixed-end boundary conditions are remarkably greater than those observed in the flexible boundary conditions, possibly due to trapping of energy inside the sand layer in the fixed-end condition.

2) Complete liquefaction was only seen in the free-field condition while only partial liquefaction (i.e. $r_u < 1$) occurred when the sand layer was overlain by a shallow foundation model (2nd series) or SDOF super-structure model (3rd series). This is mainly attributed to two main mechanisms: (1) the soil beneath and around the foundation tends to move laterally away due to the applied shear stress which causes the soil medium to dilate, resulting in a reduction of the EPWP and leads to incomplete liquefaction; and (2) increased confining pressure due to presence of shallow foundation model caused higher cyclic strength and resistance to EPWP generation increases.

3) As shaking started, the transient EPWP rapidly increased in both flexible and fixed-end conditions. However, the maximum amounts of EPWP in flexible cases were higher than those in corresponding fixed-end cases. Immediately after shaking ceased, EPWP dissipation began in both flexible and fixed-end models. A greater rate of EPWP dissipation was observed in the container with flexible boundary conditions.

4) During the initial cycles of shaking, acceleration responses were similar at various depths in both laminar and fixed-end conditions, since soil stiffness degradation was not high enough. Nevertheless, the value of acceleration peaks increased as the input wave traveled from the bottom layer to the top for the fixed-end condition in all testing series. At shallower depths, where softening of underlying soil layers was more significant, acceleration changes with time

were more noticeable. Therefore, variation of maximum acceleration responses was considerably larger especially at shallower depth for the fixed-end condition. In contrast, in the flexible condition, a relatively smooth acceleration response was captured. This difference is likely due to effects P-waves generated by reflections from fixed-end walls during shaking.

5) After the initial cycles of shaking, acceleration attenuation at the mid-height in the flexible conditions for all test series could be a sign of shear localization somewhere near the mid-height. Increasing soil softening caused higher damping ratio within the soil layer which in turn lead to significant phase lag between input and measured acceleration in all elevations. This could explain the acceleration necking after the early loading cycles in all flexible conditions. This trend is similar for the free-field condition with fixed-end boundary. However, in the second and third series with fixed-end boundaries, soil re-stiffening caused higher acceleration response after the acceleration attenuation in the early cycles of shaking.

6) Higher spectral acceleration amplitude for the fixed-end conditions was observed especially near the input motion frequency for all the cases most likely because of response amplification in the fixed-end condition due to higher energy level. The slight shift of peak spectral acceleration to the right for flexible condition curve indicates that the flexible container stiffness was lower compared to the fixed-end condition. Thus, the flexible boundary condition is closer to the actual situation and it is preferable over the fixed-end boundary in replicating free-field seismic response.

7) The captured displacement of the container laminates tracked using image processing technique for flexible tests showed that displacement values decreased from a maximum at the base layer to the lowest amount near the surface. Further, visual observations indicate that some non-uniformity in layers displacements for shallow foundation and SDOF super-structure cases near the surface. In the first couple of loading cycles, displacement of layers almost matches the base input, but immediately after, maximum layer displacement decayed to an approximately constant value.

8) Plotting the results of layers displacement obtained from image process analysis between t=1s and t=1.6s with 0.1 second time steps and t=2s to t=8s with the corresponding pore pressure build-up ratio (r_u) helps to gain a better understanding of how the soil layers behave during shaking. In the free-field condition, after t=1.2s, the displacement of the 10^{th} layer decreased significantly and relative displacement of the above layers declined to zero which

means the above layers move like a rigid body. It could be inferred that shear localization has taken place somewhere near the 10th layer. This phenomenon occurred twice for the second test series in two different times while in the third series, only one shear localization occurred near the 13rd layer. Besides, larger layer displacements for the time span of 2s<t<8s, when the foundation model exists on the soil surface (2nd and 3rd series) may be related to incomplete liquefaction compared free-field condition.

Acknowledgement

This study was funded by the IIEES under project No. AM-7/183-6321, and this support is highly appreciated. The authors would like to thank the image processing team, including Dr. Hossein Jahankhah and his team who carried out the image processing of the tests in this project.

References

Acacio, A. A., Kobayashi, Y., Towhata, I., Bautista, R. T., and Ishihara, K. 2001. "Subsidence of Building Foundation Resting Upon Liquefied Subsoil: Case Studies and Assessment." *Soils and Foundations*, 41(6), 111-128. https://doi.org/10.3208/sandf.41.6_111

Adalier, K., Elgamal, A., Meneses, J., and Baez, J. I. 2003. "Stone Columns as Liquefaction Countermeasure in Non-Plastic Silty Soils." *Soil Dynamics and Earthquake Engineering*, 23(7), 571-584. https://doi.org/10.1016/S0267-7261(03)00070-8

Alam, M. J. and Towhata, I. "Some Important Aspects of Physical Modelling of Liquefaction in 1-g Shaking Table." Paper presented at AIP Conference, Vol. 1020, No. 1, 419-425, Calabria, Italy, July 8-11, 2008. https://doi.org/10.1063/1.2963865

Bertalot, D., Brennan, A. J., and Villalobos, F. A. 2013. "Influence of Bearing Pressure on Liquefaction-Induced Settlement of Shallow Foundations." *Géotechnique*," 63(5), 391-399. http://dx.doi.org/10.1680/geot.11.P.040

Bird, J. F., Bommer, J. J., Bray, J. D., Sancio, R., and Spence, R. J. S. 2004. "Comparing Loss Estimation with Observed Damage in a Zone of Ground Failure: A Study of the 1999 Kocaeli Earthquake in Turkey." *Bulletin of Earthquake Engineering*, 2(3), 329-360. https://doi.org/10.1007/s10518-004-3804-0

Bishop, A. W., Green, G. E., Garga, V. K., Andresen, A., and Brown, J. D. 1971. "A New Ring Shear Apparatus and Its Application to the Measurement of Residual Strength." *Géotechnique*, 21(4), 273-328. https://doi.org/10.1680/geot.1971.21.4.273

Bray, J. D., Cubrinovski, M., Zupan, J., and Taylor, M. 2014. "Liquefaction Effects on Buildings in the Central Business District of Christchurch." *Earthquake Spectra*, 30(1), 85-109. https://doi.org/10.1193/022113EQS043M

Bray, J. D. and Dashti, S. 2014. "Liquefaction-Induced Building Movements." *Bulletin of Earthquake Engineering*, 12(3), 1129-1156. https://doi.org/10.1007/s10518-014-9619-8

Bray, J. D. and Luque, R. 2017. "Seismic Performance of a Building Affected by Moderate Liquefaction During the Christchurch Earthquake." *Soil Dynamics and Earthquake Engineering*, 102, 99-111. https://doi.org/10.1016/j.soildyn.2017.08.011

Bray, J. D., Stewart, J. P., Baturay, M. B., Durgunoglu, T., Onalp, A., Sancio, R. B., Stewart, J. P., Ural, D., Ansal, A., Bardet, J. B., and Barka, A. 2000. "Damage Patterns and

Foundation Performance in Adapazari." *Earthquake Spectra*, 16(S1), 163-189. https://doi.org/10.1193/1.1586152

Bullock, Z., Dashti, S., Karimi, Z., Liel, A., Porter, K., and Franke, K. 2018. "Probabilistic Models for Residual and Peak Transient Tilt of Mat-Founded Structures on Liquefiable Soils." *Journal of Geotechnical and Geoenvironmental Engineering*, 145(2), p. 04018108. https://doi.org/10.1061/(ASCE)GT.1943-5606.0002002

Dashti, S., Bray, J. D., Pestana, J. M., Riemer, M., and Wilson, D. 2010. "Centrifuge Testing to Evaluate and Mitigate Liquefaction-Induced Building Settlement Mechanisms." *Journal of Geotechnical and Geoenvironmental Engineering*, 136(7), 918-929. https://doi.org/10.1061/(ASCE)GT.1943-5606.0000306

Dashti, S., Bray, J. D., Pestana, J. M., Riemer, M., and Wilson, D. 2010. "Mechanisms of Seismically Induced Settlement of Buildings with Shallow Foundations on Liquefiable Soil." *Journal of Geotechnical and Geoenvironmental Engineering*, 136(1), 151-164. https://doi.org/10.1061/(ASCE)GT.1943-5606.0000179

Ecemis, N. 2013. "Simulation of Seismic Liquefaction: 1-g Model Testing System and Shaking Table Tests." *European Journal of Environmental and Civil Engineering*, 17(10), 899-919. https://doi.org/10.1080/19648189.2013.833140

Fiegel, G. 1994. "Effect of Model Containers on Dynamic Soil Response." Paper presented at the International Conference Centrifuge 94, 145-150, Singapore, August 31-September 2, 1994.

Fishman, K. L., Mander, J. B. and Richards Jr, R. 1995. "Laboratory Study of Seismic Free-Field Response of Sand." *Soil Dynamics and Earthquake Engineering*, 14(1), 33-43. https://doi.org/10.1016/0267-7261(94)00017-B

Forcellini, D. 2019. "Numerical Simulations of Liquefaction on an Ordinary Building During Italian (20 May 2012) Earthquake." *Bulletin of Earthquake Engineering*, 1-27. https://doi.org/10.1007/s10518-019-00666-5

Franke, K. W., Candia, G., Mayoral, J. M., Wood, C. M., Montgomery, J., Hutchinson, T., and Morales-Velez, A. C. 2019. "Observed Building Damage Patterns and Foundation Performance in Mexico City Following The 2017 M7.1 Puebla-Mexico City Earthquake." *Soil Dynamics and Earthquake Engineering*, 125, p. 105708. https://doi.org/10.1016/j.soildyn.2019.105708

García-Torres, S. and Madabhushi, G. S. P. 2019. "Performance of Vertical Drains in Liquefaction Mitigation Under Structures." *Bulletin of Earthquake Engineering*, 1-18. https://doi.org/10.1007/s10518-019-00717-x

Ghayoomi, M., Dashti, S., and McCartney, J. S. 2013. "Performance of a Transparent Flexible Shear Beam Container for Geotechnical Centrifuge Modeling of Dynamic Problems." *Soil Dynamics and Earthquake Engineering*, 53, 230-239. https://doi.org/10.1016/j.soildyn.2013.07.007

Ghayoomi, M., Dashti, S., and McCartney, J. S. 2014. "Closure to 'Performance of a Transparent Flexible Shear Beam Container for Geotechnical Centrifuge Modelling of Dynamic Problems' by Ghayoomi M., Dashti S., and McCartney J. S., Published in *Soil Dynamics and Earthquake Engineering*, 53 (2013), DOI: 10.1016/j.soildyn.2013.07.007." *Soil Dynamics and Earthquake Engineering*, 67, 363-369. https://doi.org/10.1016/j.soildyn.2014.02.002

Gibson, A. D. "Physical Scale Modeling of Geotechnical Structures at One-G." PhD diss., California Institute of Technology, 1997.

Gibson A. D. and Scott R. F. "Comparison of a 1g and Centrifuge Model Dynamic Liquefaction Test: Preliminary Results." Paper presented at the first International Conference on Earthquake Geotechnical Engineering, 773-778, Rotterdam, Netherlands, 1995.

Hayashi, K., Fujii, N., Muramatsu, T. and Houjyou, K. 1997. "Direct comparison Of Gravity Model and Centrifuge Model for The Seismic Problem (In Japanese)." *Doboku Gakkai Ronbunshu*, 582, 207-216. https://doi.org/10.2208/jscej.1997.582_207

Hayden, C. P., Zupan, J. D., Bray, J. D., Allmond, J. D., and Kutter, B. L. 2014. "Centrifuge Tests of Adjacent Mat-Supported Buildings Affected by Liquefaction." *Journal of Geotechnical and Geoenvironmental Engineering*, 141(3), p. 04014118. https://doi.org/10.1061/(ASCE)GT.1943-5606.0001253

Hung, W. Y., Lee, C. J., and Hu, L. M. 2018. "Study of The Effects of Container Boundary and Slope on Soil Liquefaction by Centrifuge Modeling." *Soil Dynamics and Earthquake Engineering*, 113, 682-697. https://doi.org/10.1016/j.soildyn.2018.02.012

Hushmand, B., Scott, R. F., and Crouse C. B. 1988. "Centrifuge Liquefaction Tests in a Laminar Box." *Géotechnique*, 38(2), 253-262. https://doi.org/10.1680/geot.1988.38.2.253

Iai, S. 1989. “Similitude for Shaking Table Tests on Soil-Structure-Fluid Model in 1g Gravitational Field.” *Soils and Foundations*, 29(1), 105-118. https://doi.org/10.3208/sandf1972.29.105

Jafarian, Y., Haddad, A., Mehrzad, B. 2016. “Load-Settlement Mechanism of Shallow Foundations Rested on Saturated Sand with Upward Seepage.” *International Journal of Geomechanics*, 17(3), p. 04016076. https://doi.org/10.1061/(ASCE)GM.1943-5622.0000777

Jafarian, Y., Javdanian, H. 2019. “Dynamic Properties of Calcareous Sand from The Persian Gulf in Comparison with Siliceous Sands Database.” *International Journal of Civil Engineering*, 1-5. https://doi.org/10.1007/s40999-019-00402-9

Jafarian, Y., Mehrzad, B., Lee, C. J., and Haddad, A. H. 2017. “Centrifuge Modeling of Seismic Foundation-Soil-Foundation Interaction on Liquefiable Sand.” *Soil Dynamics and Earthquake Engineering*, 97, 184-204. https://doi.org/10.1016/j.soildyn.2017.03.019

Jafarian, Y., Taghavizade, H., Rouhi, S., Shojaemehr, S., and Esmaeilpour, P. 2020. “Shaking Table Experiments to Evaluate the Boundary Effects on Seismic Response of Saturated and Dry Sands in Level Ground Condition.” *International Journal of Civil Engineering*, pp. 1-13. https://doi.org/10.1007/s40999-019-00485-4

Jafarian, Y., Vakili, R., Abdollahi, A. S., and Baziar, M. H. 2013. “Simplified Soil Liquefaction Assessment Based on Cumulative Kinetic Energy Density: Attenuation Law and Probabilistic Analysis.” *International Journal of Geomechanics*, 14(2), 267-281. https://doi.org/10.1061/(ASCE)GM.1943-5622.0000317

Jafarzadeh, B. “Design and Evaluation Concepts of Laminar Shear Box For 1g Shaking Table Tests,” Paper presented at the Thirteen World Conference on Earthquake Engineering, Vancouver, Canada, August 1-6, 2004.

Kagawa, T. “On the Similitude in Model Vibration Tests of Earth-Structures.” Paper presented at the Japan Society of Civil Engineers, Vol. 1978, No. 275, 69-77, Japan, 1978. https://doi.org/10.2208/jscej1969.1978.275_69

Karimi, Z. and Dashti, S. 2016. “Numerical and Centrifuge Modeling of Seismic Soil-Foundation-Structure Interaction on Liquefiable Ground.” *Journal of Geotechnical and Geoenvironmental Engineering*, 142(1), p. 04015061. https://doi.org/10.1061/(ASCE)GT.1943-5606.0001346

Karimi, Z., Dashti, S., Bullock, Z., Porter, K., and Liel, A. 2018. "Key predictors Of Structure Settlement on Liquefiable Ground: A Numerical Parametric Study." *Soil Dynamics and Earthquake Engineering*, 113, 286-308. https://doi.org/10.1016/j.soildyn.2018.03.001

Kokusho, T. and Iwatate, T. "Scaled Model Tests and Numerical Analyses on Nonlinear Dynamic Response of Soft Grounds." Paper presented at the Japan Society of Civil Engineers, Vol. 1979, No. 285, 57-67, Japan, 1979. https://doi.org/10.2208/jscej1969.1979.285_57

Kumar, R., Kasama, K., and Takahashi, A. 2020. "Reliability Assessment of The Physical Modeling of Liquefaction-Induced Effects on Shallow Foundations Considering Nonuniformity in the Centrifuge Model." *Computers and Geotechnics*, 122, p. 103558. https://doi.org/10.1016/j.compgeo.2020.103558

Lee, C. J., Wei, Y. C., and Kuo, Y. C. 2012. "Boundary Effects of a Laminar Container in Centrifuge Shaking Table Tests." *Soil Dynamics and Earthquake Engineering*, 34(1), 37-51. https://doi.org/10.1016/j.soildyn.2011.10.011

Li, Y., Zheng, S., Luo, W., Cui, J., and Chen, Q. 2020. "Design and Performance of a Laminar Shear Container for Shaking Table Tests." *Soil Dynamics and Earthquake Engineering*, 135, p. 106157. https://doi.org/10.1016/j.soildyn.2020.106157

Liu, L., Dobry, R. 1997. "Seismic Response of Shallow Foundation on Liquefiable Sand." *Journal of Geotechnical and Geoenvironmental Engineering*, 123(6), 557-567. https://doi.org/10.1061/(ASCE)1090-0241(1997)123:6(557)

Macedo, J. and Bray, J. D. 2018. "Key Trends in Liquefaction-Induced Building Settlement." *Journal of Geotechnical and Geoenvironmental Engineering*, 144(11), 04018076. https://doi.org/10.1061/(ASCE)GT.1943-5606.0001951

Maymand P. J. "Shaking table Scale Model Tests of Nonlinear Soil-Pile-Superstructure Interaction in Soft Clay." PhD diss., University of California Berkeley, 1998.

Mehrzad, B., Jafarian, Y., Lee, C. J., and Haddad, A. H. 2018. "Centrifuge Study into the Effect of Liquefaction Extent on Permanent Settlement and Seismic Response of Shallow Foundations." *Soils and foundations*, 58(1), 228-240. https://doi.org/10.1016/j.sandf.2017.12.006

Okamoto, S. "Bearing Capacity of Sandy Soil and Lateral Earth Pressure During Earthquake." Paper presented at the First World Conference on Earthquake Engineering, 1-26, California, USA, 1956.

Pamuk, A., Gallagher, P. M., and Zimmie, T. F. 2007. "Remediation of Piled Foundations Against Lateral Spreading by Passive Site Stabilization Technique." *Soil Dynamics and Earthquake Engineering*, 27, 864-874. https://doi.org/10.1016/j.soildyn.2007.01.011

Pane, V., Vecchietti, A., and Cecconi, M. 2016. "A Numerical Study on the Seismic Bearing Capacity of Shallow Foundations." *Bulletin of Earthquake Engineering*, 14(11), 2931-2958. https://doi.org/10.1007/s10518-016-9937-0

Pozo, C., Gng, Z., and Askarinejad, A. "Evaluation of Soft Boundary Effects (SBE) on the behavior of a shallow foundation." Paper presented at the Third European Conference on Physical Modelling in Geotechnics (EUROFUGE 2016*)*, 385-390, Nantes, France, 2016.

Prasad, S. K., Towhata, I., Chandradhara, G. P., and Nanjundaswamy, P. 2004. "Shaking Table Tests in Earthquake Geotechnical Engineering." *Current Science*, 1398-1404. https://www.jstor.org/stable/24109480

Shahnazari, H., Jafarian, Y., Tutunchian, M. A., and Rezvani, R. 2016. "Probabilistic Assessment of Liquefaction Occurrence in Calcareous Fill Materials of Kawaihae Harbor, Hawaii." *International Journal of Geomechanic*s, 16(6), p. 05016001. https://doi.org/10.1061/(ASCE)GM.1943-5622.0000621

Shen, C. K., Li, X. S., Ng, C. W. W., Van Laak, P. A., Kutter, B. L., and Cappel, K. "Development of a Geotechnical Centrifuge in Hong Kong." Paper presented at the International Conference Centrifuge (Centrifuge 98), Tokyo, Japan, September 23-25, 1998.

Suzuki, K., Babasaki, R., and Suzuki, Y. "Liquefaction Tests by a Laminar Box in a Centrifuge." Paper presented at the Second International Conference on Recent Advances in Geotechnical Earthquake Engineering and Soil Dynamic, 225-228, St. Louis, Missouri, USA, 1991.

Tabatabaiefar, H. R. 2016. "Detail Design and Construction Procedure of Laminar Soil Containers for Experimental Shaking Table Tests." *International Journal of Geotechnical Engineering*, 10(4), 328-336. https://doi.org/10.1080/19386362.2016.1145419

Takahashi, A., Takemura, J., Suzuki, A., and Kusakabe, O. 2001. "Development and Performance of an Active Type Shear Box in a Centrifuge." *International Journal of Physical Modelling in Geotechnics*, 1(2), 1-17.

https://doi.org/10.1680/ijpmg.2001.010201

Taucer, F., Alarcon, J. E., and So, E. 2009. "2007 August 15 Magnitude 7.9 Earthquake Near the Coast of Central Peru: Analysis and Field Mission Report." *Bulletin of Earthquake Engineering*, 7(1), 1-70. https://doi.org/10.1007/s10518-008-9092-3

Thevanayagam, S., Kanagalingam, T., Reinhorn, A., Tharmendhira, R., Dobry, R., Pitman, M., Abdoun, T., Elgamal, A., Zeghal, M., Ecemis, N., and El Shamy, U. 2009. "Laminar Box System for 1-g Physical Modeling of Liquefaction and Lateral Spreading." *Geotechnical Testing Journal*, 32(5), 438-449. https://doi.org/10.1520/GTJ102154

Tokimatsu, K., Hino, K., Suzuki, H., Ohno, K., Tamura, S., and Suzuki Y. 2019. "Liquefaction-Induced Settlement and Tilting of Buildings with Shallow Foundations Based on Field and Laboratory Observation." *Soil Dynamics and Earthquake Engineering*, 124, 268-279. https://doi.org/10.1016/j.soildyn.2018.04.054

Tokimatsu, K., Kojima, J., Kuwayama, S., Abe, A., and Midorikawa, S. 1994. "Liquefaction-Induced Damage to Buildings in 1990 Luzon Earthquake." *Journal of Geotechnical Engineering*, 120(2), 290-307. https://doi.org/10.1061/(ASCE)0733-9410(1994)120:2(290)

Tokimatsu, K., Tamura, S., Suzuki, H., and Katsumata, K. 2012. "Building Damage Associated with Geotechnical Problems in the 2011 Tohoku Pacific Earthquake." *Soils and Foundations*, 52(5), 956-974. https://doi.org/10.1016/j.sandf.2012.11.014

Towhata, I. 2007. *Earthquake Geotechnical Engineering*. Springer, Berlin. ISBN 978-3-540-35783-4

Toyota, H., Towhata, I., Imamura, S. I., and Kudo, K. I. 2004. "Shaking Table Tests on Flow Dynamics in Liquefied Slope." *Soils and Foundations*, 44(5), 67-84. https://doi.org/10.3208/sandf.44.5_67

Turan, A., Hinchberger, S. D., and El Naggar, H. 2009. "Design and Commissioning of a Laminar Soil Container for Use on Small Shaking tables." *Soil Dynamics and Earthquake Engineering*, 29(2), 404-414. https://doi.org/10.1016/j.soildyn.2008.04.003

Ueng, T. S., Wang, M. H., Chen, M. H., Chen, C. H., and Peng, L. H. 2006. "A large Biaxial Shear Box for Shaking Table Test on Saturated Sand." *Geotechnical Testing Journal*, 29(1), 1-8. https://doi.org/10.1520/GTJ12649

Van Laak, P. A., Taboada, V. M., Dobry, R., and Elgamal, A. "Earthquake Centrifuge

Modeling Using a Laminar Box." Paper presented at the Dynamic Geotechnical Testing II, ed. R. Ebelhar, V. Drnevich, and B. Kutter (West Conshohocken, PA: ASTM International), 370-384, 1994.

Vargas-Monge, W. "Ring Shear Tests on Large Deformation of Sand," PhD diss., University of Tokyo, 1998.

Whitman, R. V., and Lambe, P. C. 1986. "Effect of Boundary Conditions Upon Centrifuge Experiments Using Ground Motion Simulation." *Geotechnical Testing Journal*, 9(2), 61-71. https://doi.org/10.1520/GTJ11031J

Yoshida, N., Tokimatsu, K., Yasuda, S., Kokusho, T., and Okimura, T. 2001. "Geotechnical Aspects of Damage in Adapazari City During 1999 Kocaeli, Turkey Earthquake." *Soils and foundations*, 41(4), 25-45. https://doi.org/10.3208/sandf.41.4_25

Yoshimi, Y. and Tokimatsu, K. 1977. "Settlement of Buildings on Saturated Sand During Earthquakes." *Soils and Foundations*," 17(1), 23-38. https://doi.org/10.3208/sandf1972.17.23

Zayed, M., Luo, L., Kim, K., McCartney, J. S., and Elgamal, A. "Development and Performance of a Laminar Container for Seismic Centrifuge Modeling." Paper presented at the Third International Conference on Performance-Based Design in Earthquake Geotechnical Engineering (PBD-III), Vancouver, Canada, 2017.

Zhang, L. L., Zhang, L. M. and Tang, W. H. 2008. "Similarity of Soil Variability in Centrifuge Models." *Canadian geotechnical journal*, 45(8), 1118-1129. https://doi.org/10.1139/T08-066

Zeng, X. and Schofield, A. N. 1996. "Design and Performance of an Equivalent-Shear-Beam Container for Earthquake Centrifuge Modelling." *Géotechnique*, *46*(1), 83-102. https://doi.org/10.1680/geot.1996.46.1.83

List of Tables

Table 1 Summary of the laminar shear containers employed in previous studies

Table 2 IIEES laminar shear container properties

Table 3 Similitude factors

Table 4 Summary of the shaking table tests and input motion characteristics

Table 5 Properties of structure models (parameters are in model scale)

List of Figures

Fig. 1 Boundary conditions during 1D shaking, (a) in a semi-infinite half-space, (b) in a rigid smooth end wall container

Fig. 2 Schematic view of the designed laminar shear container (dimensions are in mm); (a) overall view of the container fastened on the shaking table, (b) top view of the container in deformed shape, (c) laminate (frame) plan view, (d) container elevation view, (e) section A-A longitudinal I-beam, (f) section B-B transverse I-beam

Fig. 3 Grain size distribution for Babolsar sand

Fig. 4 Input motion for all tests

Fig. 5 Structure models; (a) shallow foundation, (b) SDOF super-structure on shallow foundation

Fig. 6 Instrumentation layout (dimensions are in mm); (a) free-field with flexible boundary, (b) free-field with fixed-end boundary, (c) shallow foundation with flexible boundary, (d) shallow foundation with foxed-end boundary, (e) SDOF super-structure on shallow foundation with flexible boundary, (f) SDOF Super-structure on foundation with fixed-end boundary

Fig. 7 Comparison of acceleration responses at surface center and surface right-end for free-field sand layers in saturated and dry conditions; (a) entire shaking duration (saturated), (b) entire shaking duration (dry), (c) shaking from 0.5 to 2.5s (saturated), (d) shaking from 0.5 to 2.5s (dry), (e) spectral acceleration (saturated), (f) spectral acceleration (dry)

Fig. 8 Recorded time history of EPWP at mid-height and model base and settlement at the surface of a saturated sand layer for both flexible and fixed-end boundary conditions; (a) free-field, (b) shallow foundation, (c) SDOF on shallow foundation

Fig. 9 Recorded acceleration time history at different locations for both flexible and fixed-end boundary condition; (a) free-field, (b) shallow foundation, (c) SDOF on shallow foundation

Fig. 10 Spectral acceleration (5% damping) at different locations for both flexible and fixed-end boundary conditions; (a) free-field, (b) shallow foundation, (c) SDOF on shallow foundation

Fig. 11 Image processing technique used for capturing displacements; (a) SDOF on shallow foundation, (b) shallow foundation, (c) container layers

Fig. 12 Horizontal displacement of selected container layers obtained from image processing during shaking; (a) free-field, (b) shallow foundation, (c) SDOF on shallow foundation.

Fig. 13 Horizontal displacement of container layers obtained from image processing during shaking regarding pore water pressure generation ratio (r_u); (a) free-field from t=1s to t=1.6s, (b) free-field from t=2s to t=8s, (c) shallow foundation from t=1s to t=1.6s, (d) shallow foundation from t=2s to t=8s, (e) SDOF on shallow foundation from t=1s to t=1.6s, (f) SDOF on shallow foundation from t=2s to t=8s

949 # TABLES

950 **Table 1** Summary of the laminar shear containers employed in previous studies

Shape	Shaking	L×W×H* [mm]	L/H or D/H*	1g/Ng	Design note	Reference
Square	uniaxial	350×350×350	1.46	Ng	Stack of silicone-oiled laminates without bearings	Suzuki et al. (1991)
Rectangular	uniaxial	457×254×254	1.8	Ng	Stack of laminates separated by bearings	Van Lak et al. (1994)
Rectangular	uniaxial	900×350×470	1.9	1g	Stack of laminates separated by bearings	Gibson (1997)
Circular	biaxial	2280×2130 (D×H)	1.1	1g	Container hanging on the top laminates supported by a frame	Meymand (1998)
Polygonal (12-sided)	biaxial	584×500 (D×H)	1.17	Ng	Stack of laminates separated by bearings	Shen et al. (1998)
Rectangular	uniaxial	1000×500×1000	1	1g	Stack of laminates separated by bearings	Prasad et al. (2004)
Square	biaxial	1000×1000×1000	1	1g	Stack of laminates separated by ball bearings	Jafarzadeh (2004)
Rectangular	uniaxial	710×355×355	2	Ng	Stack of laminates separated by bearings	Pamuk et al. (2007)
Rectangular	biaxial	1888×1888×1520	1.2	1g	Laminates supported by a frame to move independently	Ueng et al. (2006)
Polygonal (8-sided)	biaxial	5000×2750×3210	0.81	1g	Ball bearings placed between the laminates	Thevanayagam et al. (2009)
Rectangular	uniaxial	900×450×807	1.1	1g	Individually supported laminates connected to an external frame	Turan et al. (2009)
Rectangular	uniaxial	1800×600×1500	1.2	1g	Stack of aluminum laminates separated by rollers	Ecemis (2013)
Rectangular	uniaxial	2100×1300×1100	1.6	1g	Stack of laminates separated by rubber layers	Tabatabaiefar (2016)
Rectangular	uniaxial	381×241×266	1.4	Ng	Individually-mounted laminates to an external frame to slide independently	Zayed et al. (2017)

* L, W, H, and D stand for length, width, height, and diameter, respectively

951

Table 2 IIEES laminar shear container properties

Geometric/ physical properties	Description		
Outer dimension	L=500 mm	W=334 mm	H=263 mm
Inner dimension	L=365 mm	W=243 mm	H=263 mm
No. of frames	18 (including one fixed laminate at the base)		
Box-to-soil mass ratio	0.24 (with assumption of ρ_s = 2 ton/m^3 for soil media) *		
Inter-layer friction coefficient	0.01		
Approximate weight (kg)	62.2/15.6 (full/empty)		

* ρ_s is mass density of soil media

Table 3 Similitude factors

Parameter	**Scaling factor (Iai 1989)**	**Prototype**
Length	N	1
Density	1	1
Strain	1	1
Mass	N^3	1
Acceleration	1	1
Velocity	$\mathrm{N}^{\frac{1}{2}}$	1
Stress	N	1
Modulus	N	1
Stiffness	N^2	1
Force	N^3	1
Shaking time	$\mathrm{N}^{\frac{1}{2}}$	1
Frequency	$\mathrm{N}^{-\frac{1}{2}}$	1

Table 4 Summary of the shaking table tests and input motion characteristics

Test series	Test ID*	Test description	Boundary condition	Soil condition	D_r (%)	Input Motion	
						Freq. (Hz)	Acc. amp. (g)
Preliminary tests	PFFD	Free-field	Laminar	Dry	30	10	0.3
	PFFS	Free-field	Laminar	Saturated	30	10	0.3
1st series	FFL	Free field	Laminar	Saturated	30	10	0.3
	FFR	Free field	Rigid	Saturated	30	10	0.3
2nd series	SFL	Shallow foundation	Laminar	Saturated	30	10	0.3
	SFR	Shallow foundation	Rigid	Saturated	30	10	0.3
3rd series	SSFL	S. Foundation + SDOF	Laminar	Saturated	30	10	0.3
	SSFR	S. Foundation + SDOF	Rigid	Saturated	30	10	0.3

* PFFD: preliminary free-field on dry sand; PFFS: preliminary free-field on saturated sand; FFL: free-field on saturated sand with flexible boundary; FFR: free-field on saturated sand with fixed-end boundary; SFL: shallow foundation on saturated sand with flexible boundary; SFR: shallow foundation on saturated sand with fixed-end boundary; SSFL: shallow foundation with SDOF super-structure on saturated sand with flexible boundary; SSFR: shallow foundation with SDOF super-structure on saturated sand with fixed-end boundary

Table 5 Properties of structure models (parameters are in model scale)

Parameters	Shallow foundation	Shallow foundation with SDOF super-structure	
		SDOF super-structure	Shallow foundation
Length (mm)	240	240	240
Width (mm)	60	40 (diameter)	60
Height (mm)	31	60	6
Mass (gr)	3516	3117.1	533.7
Contact pressure[*] (kPa)	39.9	35.4[**]	6.1[**]
Young modulus E (kPa)	2.1×10^6	2.1×10^6	2.1×10^6

[*] In prototype scale

[**] Total contact pressure of shallow foundation with SDOF super-structure is 41.5 kPa (35.4+6.1)

FIGURES

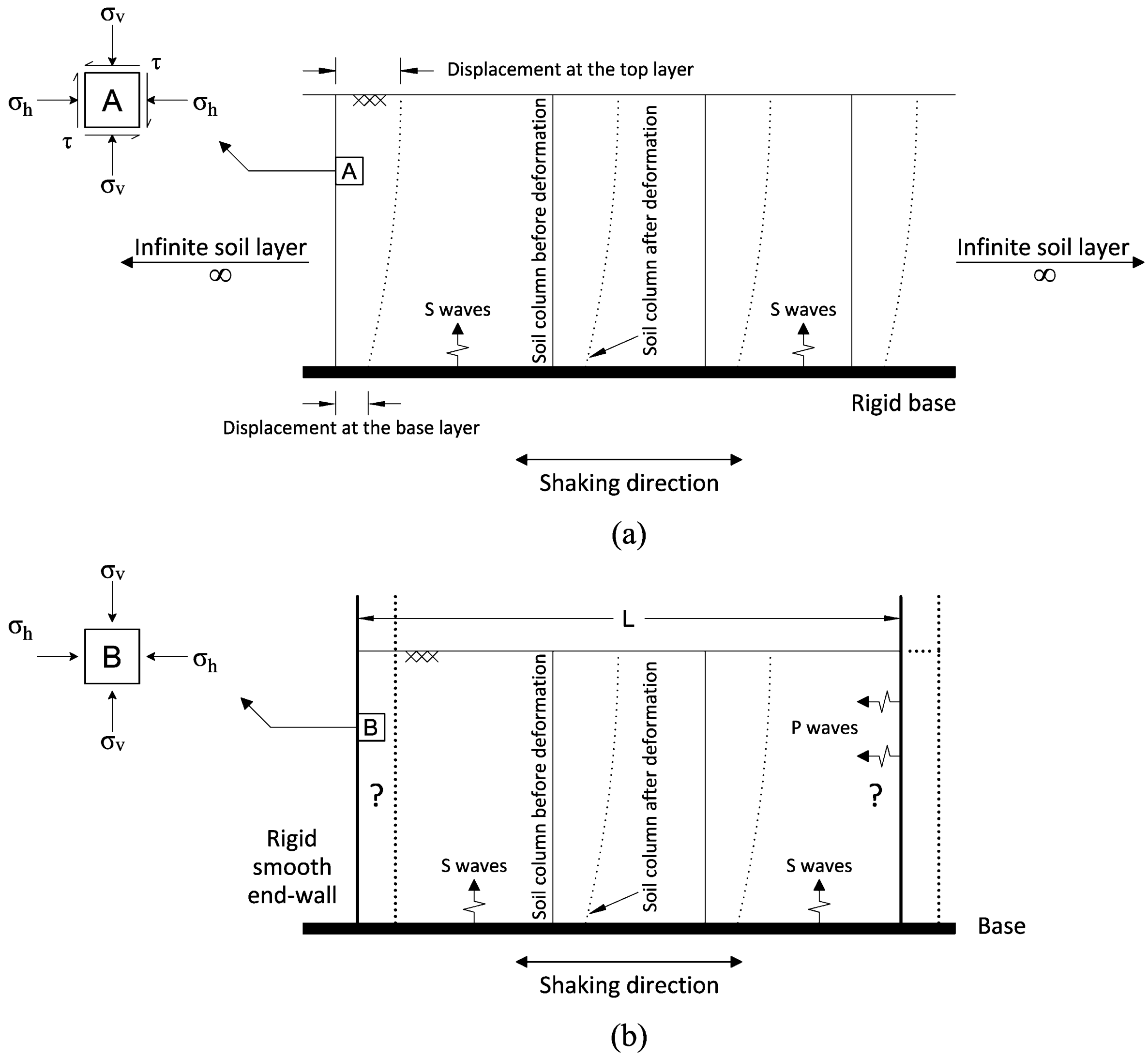

Fig. 1 Boundary conditions during 1D shaking; (a) in a semi-infinite half-space, (b) in a rigid smooth end wall container

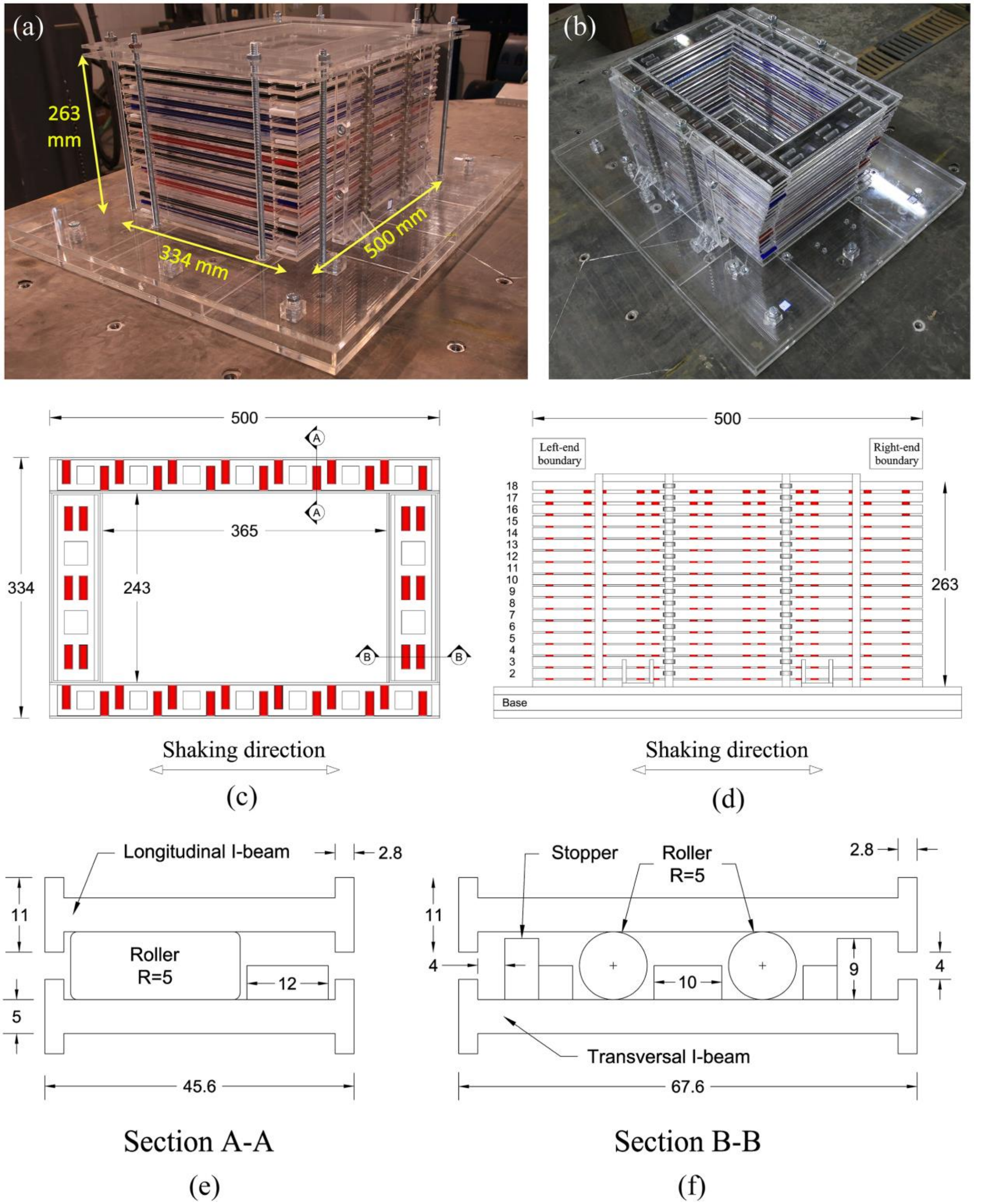

Fig. 2 Schematic view of the designed laminar shear container (dimensions are in mm); (a) overall view of the container fastened on the shaking table, (b) top view of the container in deformed shape, (c) laminate (frame) plan view, (d) container elevation view (e) section A-A longitudinal I-beam, (f) section B-B transverse I-beam

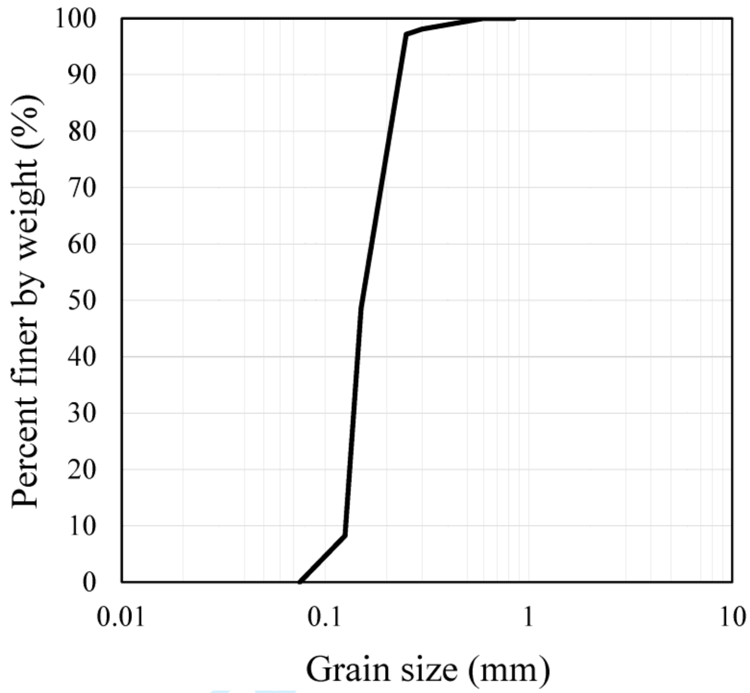

Fig. 3 Grain size distribution for Babolsar sand

Base motion	Harmonic (sine wave)
Frequency (Hz)	10
Acceleration amplitude (g)	~ 0.3
Duration	8 seconds

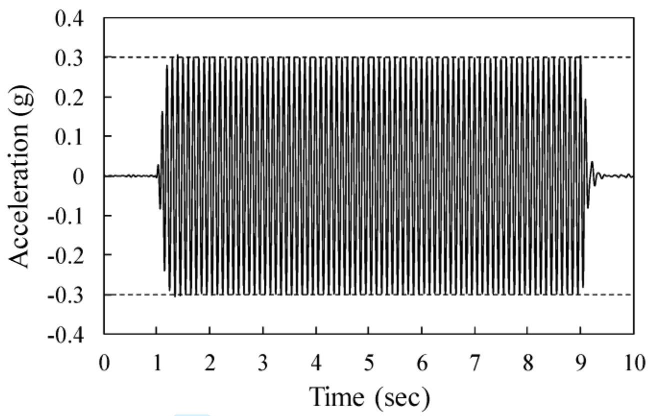

Fig. 4 Input motion for all tests

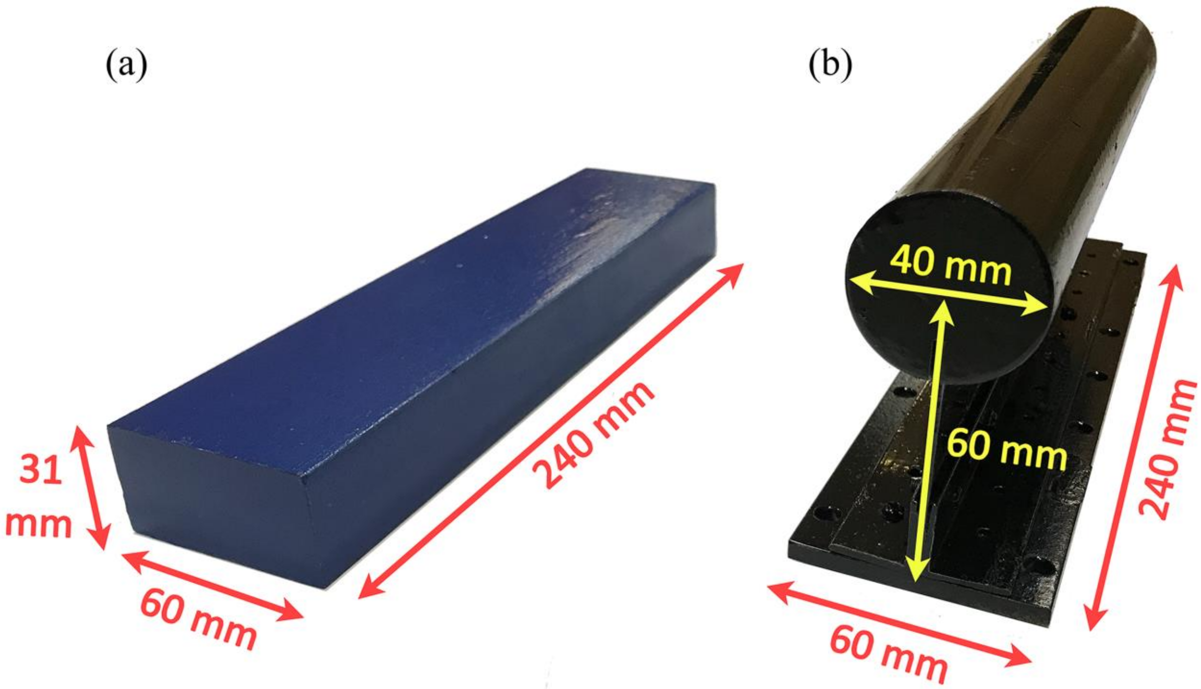

Fig. 5 Structure models; (a) shallow foundation, (b) SDOF super-structure on shallow foundation

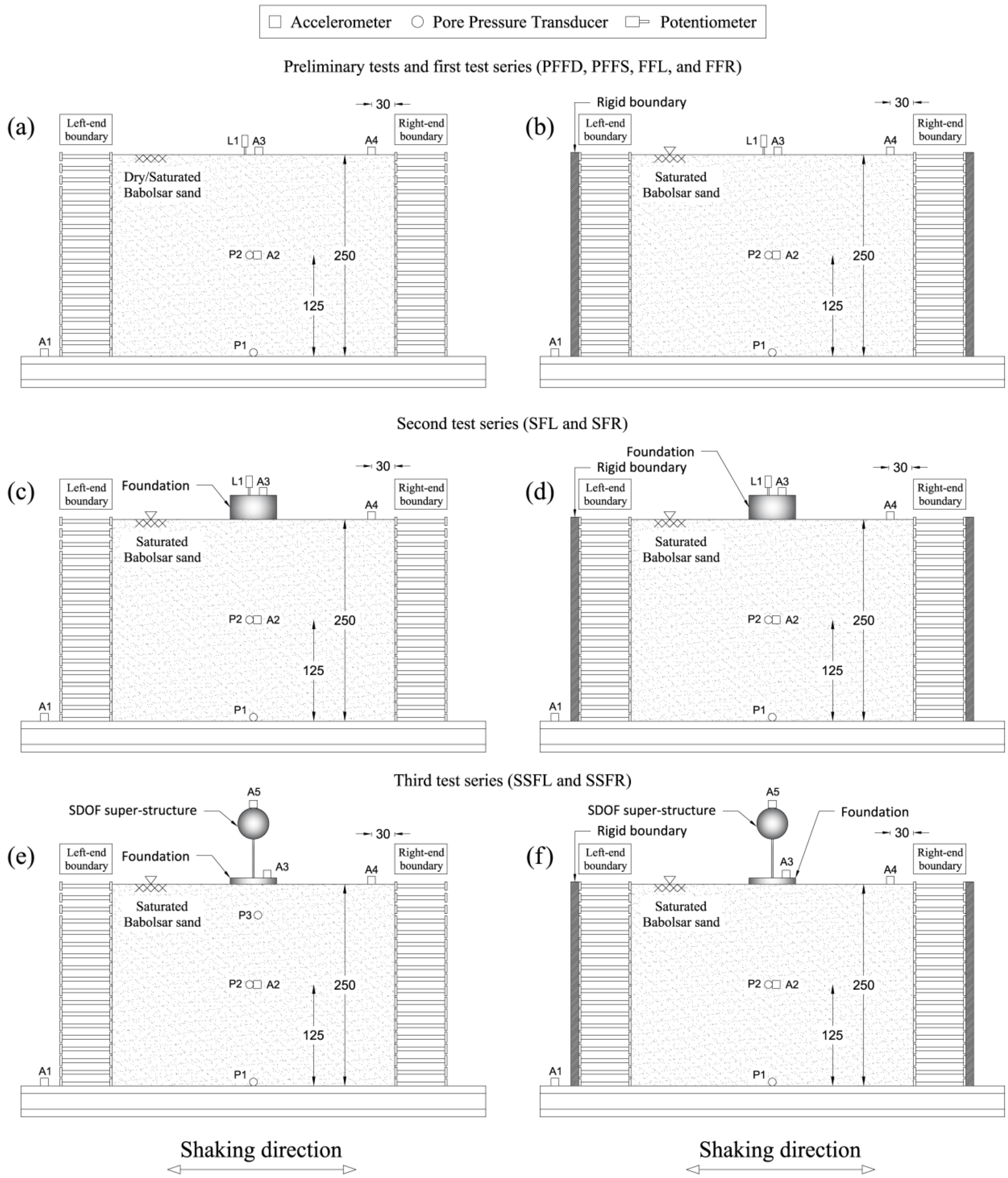

Fig. 6 Instrumentation layout (dimensions are in mm); (a) free-field with flexible boundary, (b) free-field with fixed-end boundary, (c) shallow foundation with flexible boundary, (d) shallow foundation with foxed-end boundary, (e) SDOF super-structure on shallow foundation with flexible boundary, (f) SDOF Super-structure on foundation with fixed-end boundary

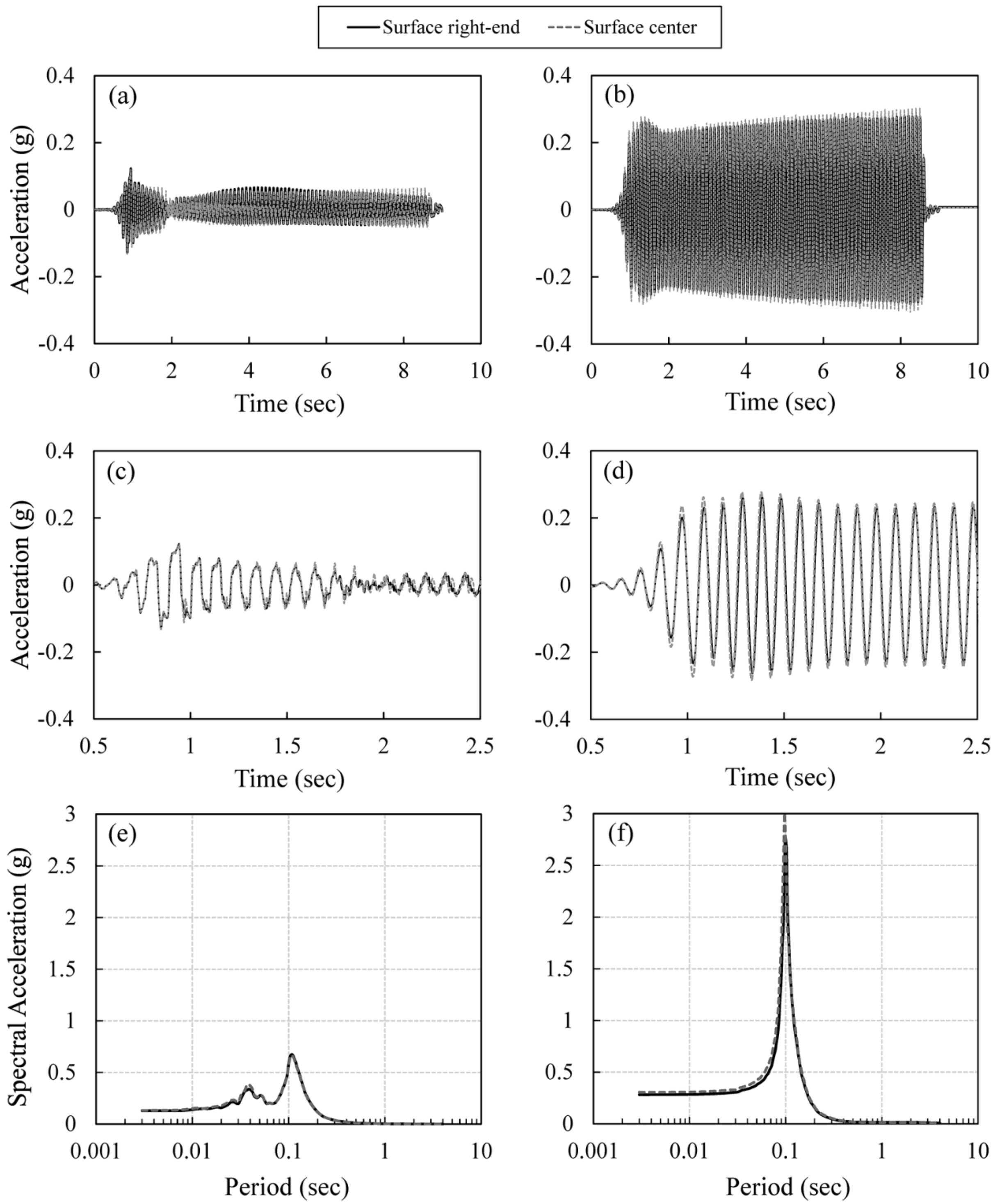

Fig. 7 Comparison of acceleration responses at surface center and surface right-end for free-field sand layers in saturated and dry conditions; (a) entire shaking duration (saturated), (b) entire shaking duration (dry), (c) shaking from 0.5 to 2.5s (saturated), (d) shaking from 0.5 to 2.5s (dry), (e) spectral acceleration (saturated), (f) spectral acceleration (dry)

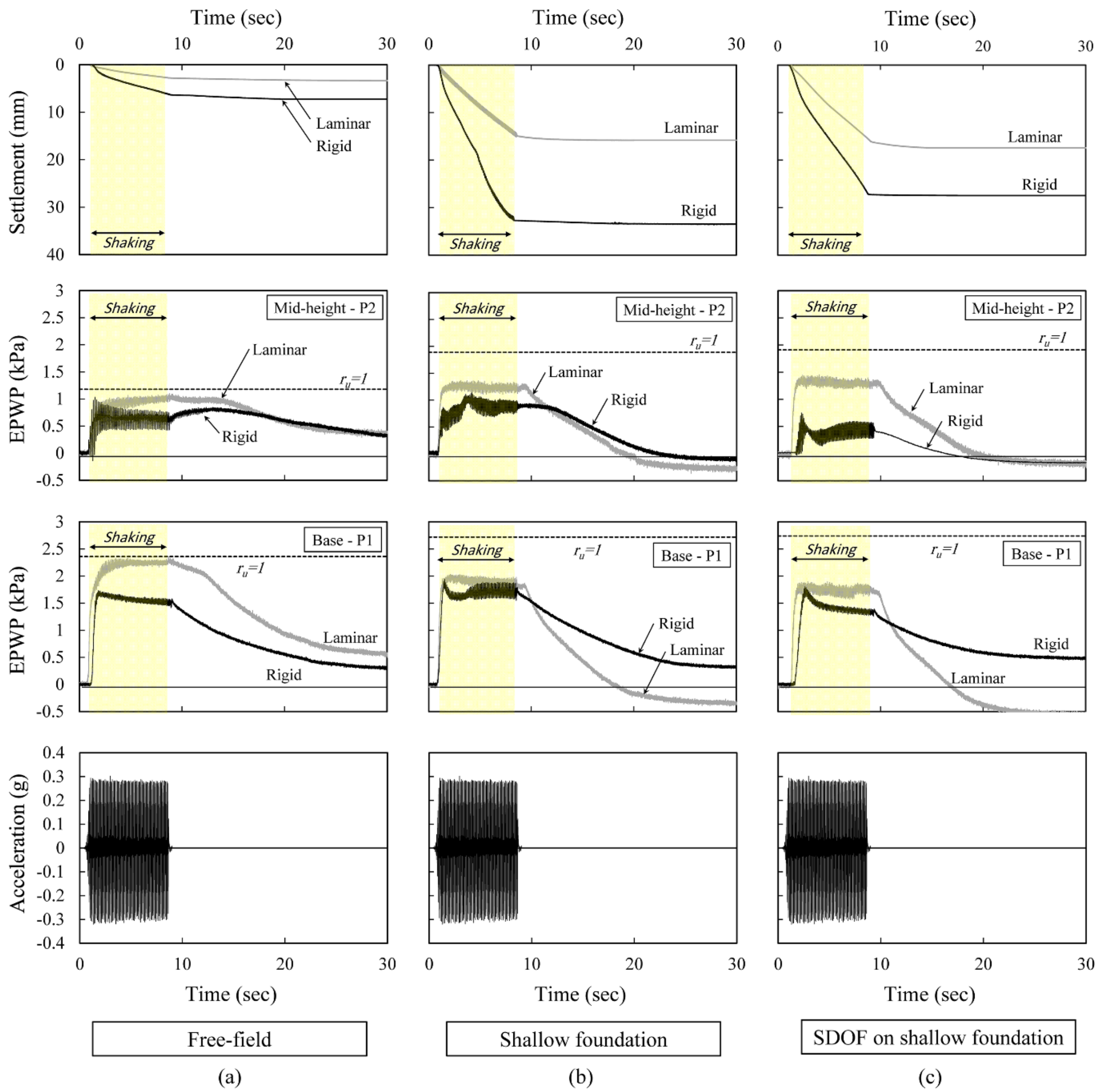

Fig. 8 Recorded time history of EPWP at mid-height and model base and settlement at the surface of a saturated sand layer for both flexible and fixed-end boundary conditions; (a) free-field, (b) shallow foundation, (c) SDOF on shallow foundation

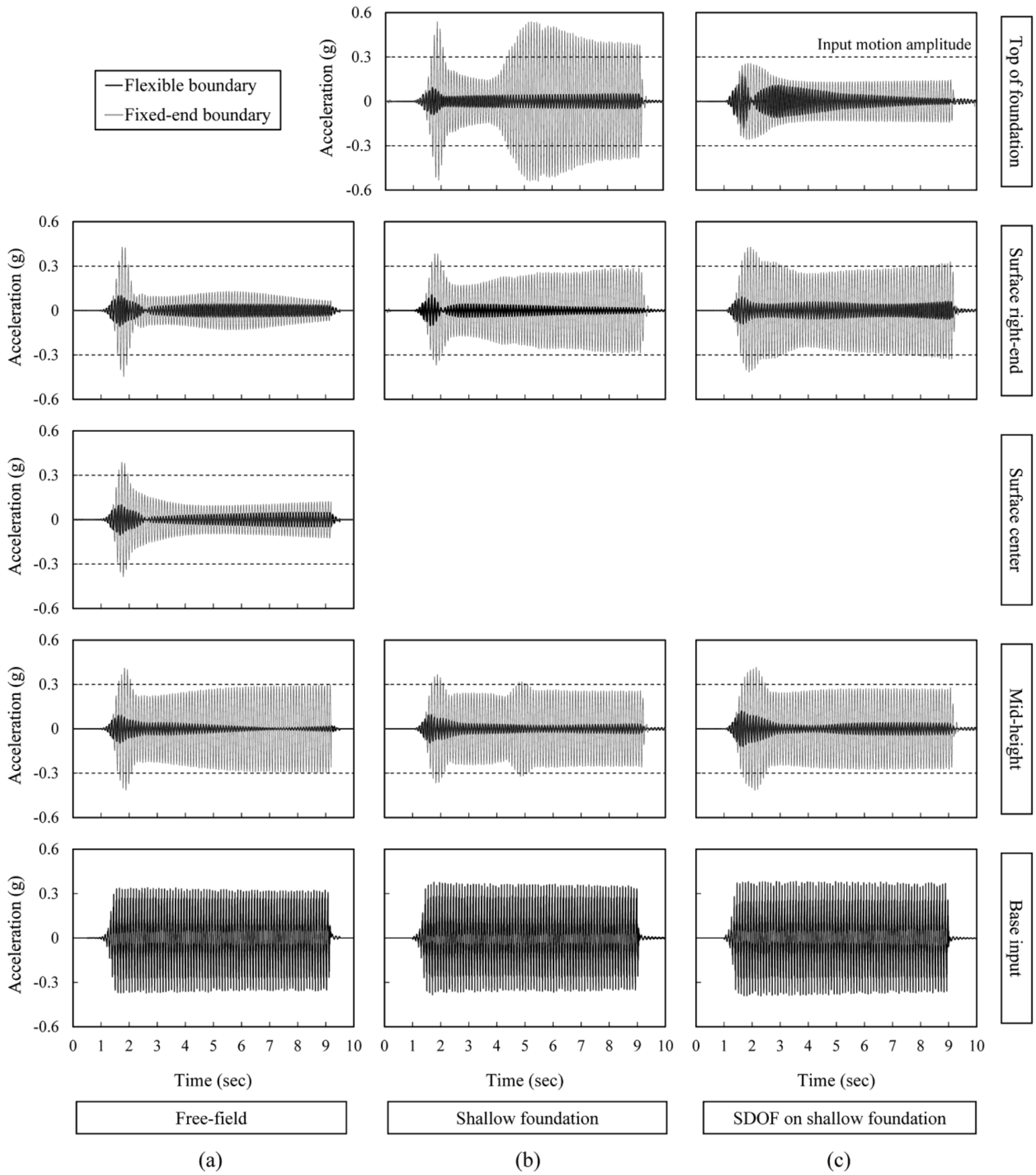

Fig. 9 Recorded acceleration time history at different locations for both flexible and fixed-end boundary condition; (a) free-field, (b) shallow foundation, (c) SDOF on shallow foundation

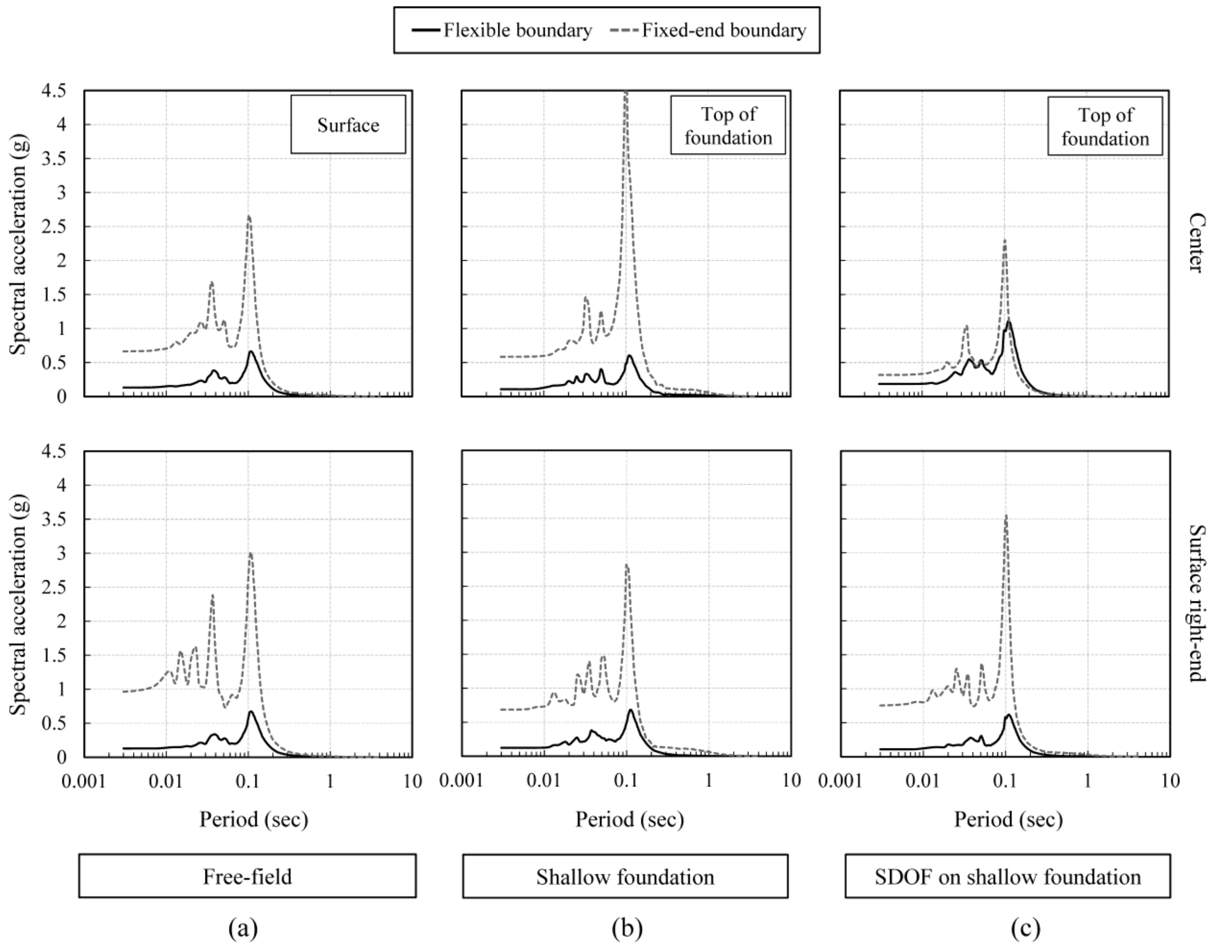

Fig. 10 Spectral acceleration (5% damping) at different locations for both flexible and fixed-end boundary conditions; (a) free-field, (b) shallow foundation, (c) SDOF on shallow foundation

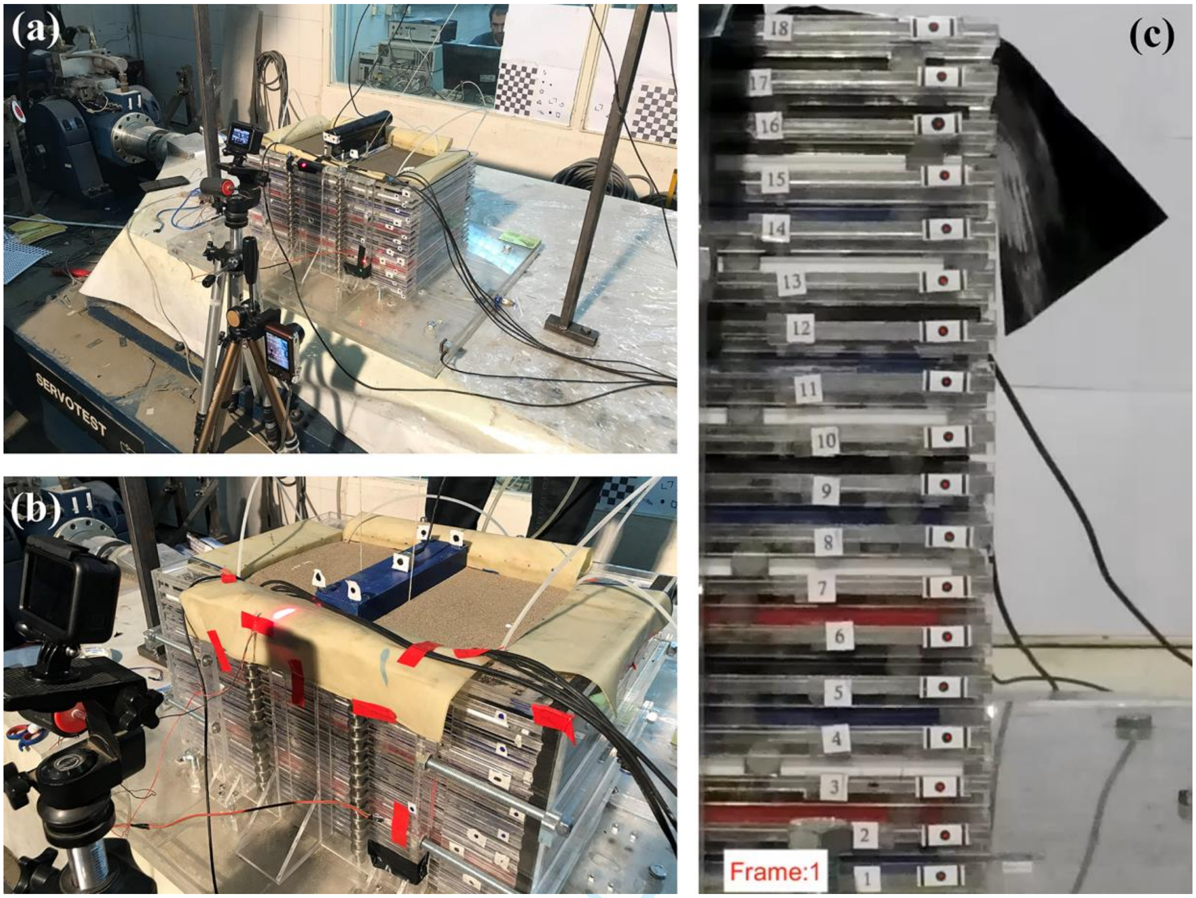

Fig. 11 Image processing technique used for capturing displacements: (a) SDOF on shallow foundation; (b) shallow foundation; (c) container layers

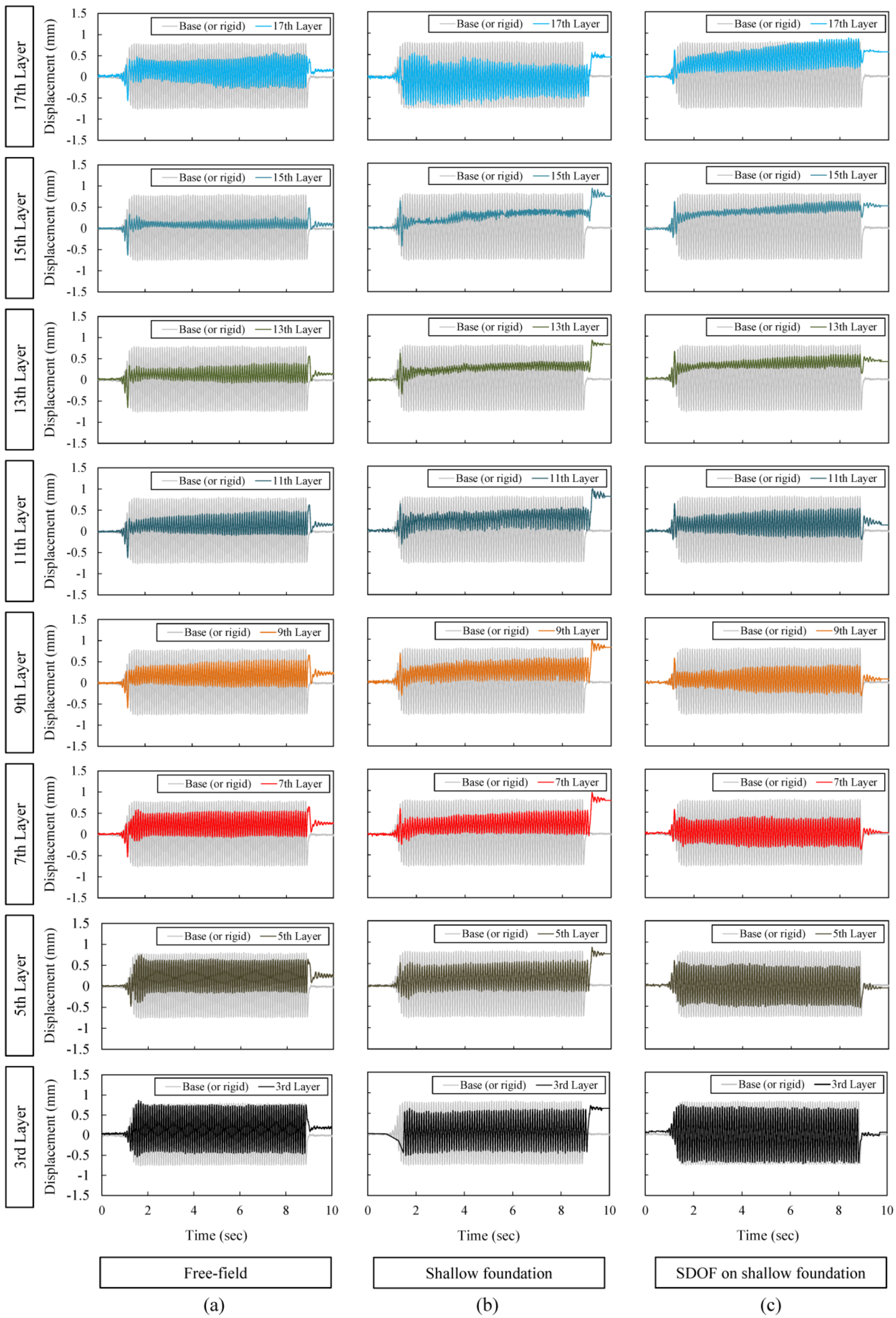
17th Layer
15th Layer
13th Layer
11th Layer
9th Layer
7th Layer
5th Layer
3rd Layer
Displacement (mm)
Base (or rigid)
Time (sec)
Free-field
Shallow foundation
SDOF on shallow foundation
(a)
(b)
(c)

Fig. 12 Horizontal displacement of selected container layers obtained from image processing during shaking: (a) free-field; (b) shallow foundation; (c) SDOF on shallow foundation.

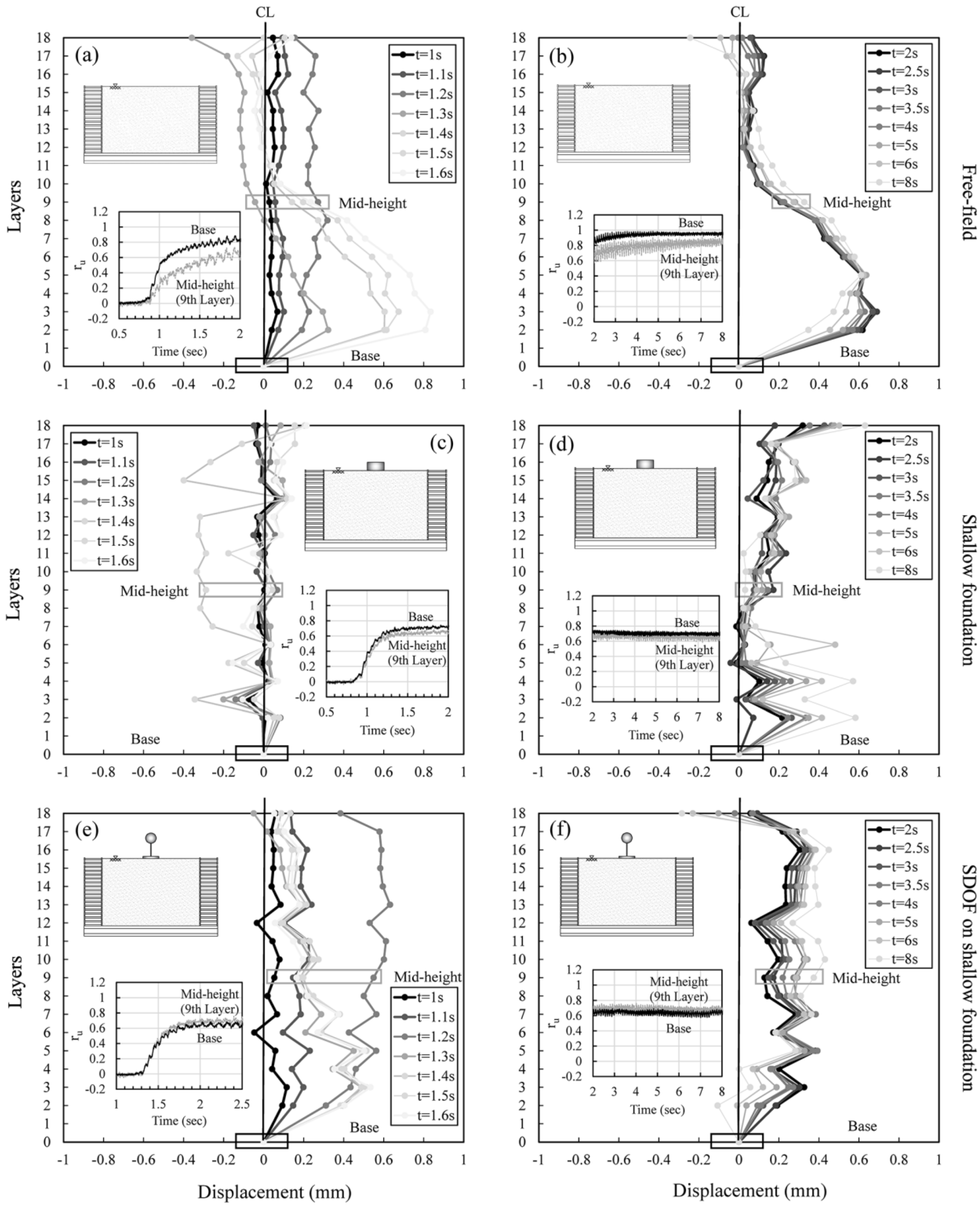

Fig. 13 Horizontal displacement of container layers obtained from image processing during shaking regarding pore water pressure generation ratio (r_u): (a) free-field from t=1s to t=1.6s; (b) free-field from t=2s to t=8s; (c) shallow foundation from t=1s to t=1.6s; (d) shallow foundation from t=2s to t=8s; (e) SDOF on shallow foundation from t=1s to t=1.6s; (f) SDOF on shallow foundation from t=2s to t=8s